ANALYSIS OF AN OSCILLATING SQUEEZE FILM
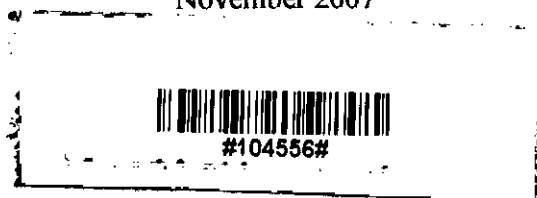# BETWEEN A RUBBER SURFACE AND A RIGID
SURFACE

A thesis submitted by

MUHANNAD MUSTAFA

In partial fulfilment of the requirements for the degree of
MASTER OF SCIENCE IN MECHANICAL ENGINEERING

DEPARTMENT OF MECHANICAL ENGINEERING
BANGLADESH UNIVERSITY OF ENGINEERING & TECHNOLOGY
Dhaka 1000, Bangladesh

November 2007

The thesis titled 'ANALYSIS OF AN OSCILLATING SQUEEZE FILM BETWEEN A RUBBER SURFACE AND A RIGID SURFACE', submitted by Muhannad Mustafa, Roll No. 100510002P, Session October 2005, has been accepted as satisfactory in partial fulfilment of the requirement for the degree of **Master of Science in Mechanical Engineering** on November 28, 2007.

BOARD OF EXAMINERS

Dr. Muhammed Mahbubur Razzaque
Associate Professor
Department of Mechanical Engineering
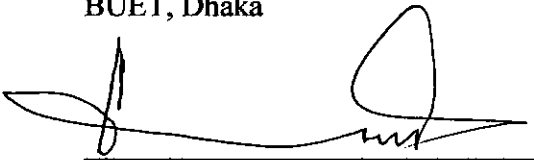BUET, Dhaka

Chairman
(Supervisor)

Dr. Md. Afsar Ali
Associate Professor
Department of Mechanical Engineering
BUET, Dhaka

Member

Dr. M. Maksud Helali
Professor and Head
Department of Mechanical Engineering
BUET, Dhaka

Member
(Ex-officio)

Dr. Gazi Md. Khalil
Professor
Department of Naval Architecture and Marine Engineering
and Dean
Faculty of Mechanical Engineering
BUET, Dhaka

Member
(External)

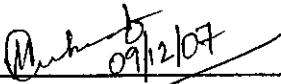# TABLE OF CONTENTS

CANDIDATE'S DECLARATION

It is hereby declared that this thesis or any part of it has not been submitted elsewhere for the award of any degree or diploma.

Muhannad Mustafa

ACKNOWLEDGMENT

LIST OF FIGURES

LIST OF TABLES

Nomenclature

Roman symbols:

a_s	Amplitude of oscillation (mm)
D	Diameter of rubber block
f	Frequency (Hz)
F	Hydrodynamic film force (N)
h	Film thickness (mm)
$\dot{h}$	Oscillating velocity (m/sec)
h_{min}	Minimum film thickness (mm)
$h_{n.clearance}$	Net clearance (mm)
h_0	Initial film thickness (mm)
$\bar{h}$	Arithmetic mean of film thickness (mm)
ID	Inner diameter (mm)
k	Permeability (m^2)
L	Thickness of rubber block
m	Arithmetic mean of surface height (mm)
OD	Outer diameter (mm)
P_T	Pressure generated in fluid film and porous matrix (Pa)
p	Fluid film pressure (Pa)
p_m	Pressure in porous matrix (Pa)
p_1, q_0, q_1	Coefficients in constitutive equations (Second, MPa and kPa-s respectively)
Q_r	Radial leakage flow from the film region through the clearance gap (m^3/sec)
Q_p	Axial leakage flow from the clearance gap into the porous matrix (m^3/sec)
Q	Net leakage flow rate in radial direction (l/sec or cc/sec)
r	Distance in the radial direction (mm)
r_a	Radius of rubber block (mm)
Re_s	Squeeze Reynolds number
T	Dimensionless Time
t	Absolute Time (Second)
$\dot{V}$	variation in volume of the clearance gap with time (m^3/sec)
v_{rm}	Average velocity in radial direction (m/sec)

Greek symbols:

β^*	Auto correlation length (mm)
δ_s	Viscoelastic deformation of rubber surface (mm)
ε	Strain (mm/mm)
η	Absolute Viscosity (Pa.s)
μ	Standard deviation of surface height of rubber block (mm)

ρ	Density (kg/m^3)
σ	Normal stress (Pa)
ξ	inlet loss coefficient

Subscripts:

i,j	Nodal points along row and column of matrix
m	Porous matrix
o	Initial value

Abbreviation:

ACF	Auto-correlation function
ACL	Auto-correlation length (mm)
CLA	Center line average (mm)

Abstract

Squeeze film theories have often been a major area of interest in fluid mechanics. In the present thesis, effects of surface roughness and permeability of rubber block on leakage flow rate and hydrodynamic force developed in fluid film between a cylindrical rigid surface and a cylindrical rubber surface are analyzed. The modified Reynolds equation, Laplace equation and governing equation for three parameter viscoelastic model are solved simultaneously to obtain pressure developed in fluid film between the mating surfaces as well as in the porous matrix and viscoelastic deformation of rubber surface. Equations are discretized into finite difference equations and solved by Gauss-Siedel iteration. It is seen that with increasing standard deviation and center line average (CLA) of surface height of rubber block, load carrying capacity increases significantly developing huge hydrodynamic force in the fluid film. Leakage flow rate also decreases with increasing standard deviation and center line average (CLA) of surface height of rubber block. Whereas with increasing permeability of rubber block, load carrying capacity decreases significantly but leakage flow rate decreases slightly. The present analyses contribute to designing many engineering applications such as bearing, wet clutch and non-contacting face seal. The results obtained from the present model are compared with experimental results available in the literature and a very good agreement is found.
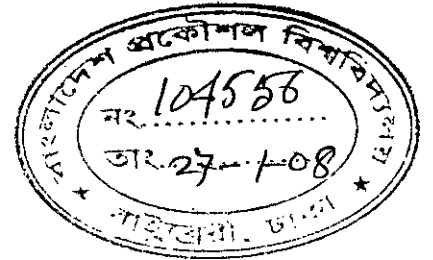
Chapter 1

Introduction

1.1 Introduction

The squeeze film theories are being extensively explored by the biomedical engineers for the studies of synovial joints, by the computer hardware engineers for the study of thin film lubrication in hard disks and by the physicists and chemists for the study of coalescence in multiphase flows. The analysis of squeeze film, in particular, between a porous rubber block and an oscillating rigid plate has long been a subject of research in connection to the studies of bearings, wet-clutches, snow tires, non-contacting mechanical face seals, gaskets, thrust washers, O-rings, printing processes, etc. When a soft permeable material like a porous rubber is used for bearing surfaces, the hydrodynamic force is induced by the relative motion of the mating surfaces as in the case of ordinary bearings with impermeable (nonporous) surfaces. The bearings with permeable surfaces will yield a smaller magnitude of hydrodynamic force and lower load-carrying capacity than the impermeable surface bearings due to the seepage flow through the permeable material. These characteristics seem to be unfavorable from the viewpoint of ordinary bearing performance. However, the penetration flow through the porous matrix and the deformation of the surface due to the hydrodynamic force becomes attractive characteristics for some applications such as wet clutches and snow tires. For wet clutches, the penetration flow across the surface could attenuate the variation of fluid-film pressures in the engagement and disengagement processes of the friction plate and could contribute to a reduction of temperature rise between the mating surfaces. For rubber tires the permeable surface facilitates pumping out of the liquid film

formed between the tire and road and thereby prevents the viscous hydroplaning phenomena.

Moreover, the deformable surface has advantages over the rigid surface due to its tolerances to misalignment in the bearing system, foreign particles in lubricants, etc. Mechanical seals are widely used in pumps, compressors, turbo-machinery and powered vessels. Non-contacting face seals [Appendix A] provide longer life but at the cost of some leakage. In these types of seals, reason of failure is not always clear and may be attributed to the process, operation, design or their combination. Nevertheless, the most probable cause of non-contacting seal failure is the occurrence of some undesired intermittent contact between the seal faces which occurs due to vibration. Therefore, contact elimination as well as decreasing leakage flow in non-contacting face seals are of prime importance, especially in critical applications (such as nuclear reactor cooling pumps) where seal failure may have severe implications. Emphasis was given on analysis of dynamic behavior of squeeze film between the mating surfaces in seals under oscillating motion after the disaster of space shuttle *Challenger* occurred in 1986 due to seal failure resulting from huge vibration.

In the present thesis, effects of surface roughness and permeability of rubber materials on squeeze film between rubber block and rigid surface are studied. It is shown that rough surface of rubber material often contributes to good load carrying capacity which is important for wet clutch and bearing applications and also minimizes leakage flow which is favorable for sealing applications.

1.2 Earlier Research Works

Early researchers investigated the hydrodynamic behavior of squeeze films associated with porous media. Sneak (1968) showed that misalignment and surface waviness affect face seal performance in the same order the clearance affects the performance of aligned seal surfaces. It was found that variations in surface flatness which are likely to occur

during manufacturing process or as a result of thermal distortion can result in increase in leakage rate. Waviness and misalignment are found to have negligible effect on separating force in absence of cavitation. Then Cheng *et al.* (1968) did extensive research on the behavior of hydrostatic and hydrodynamic non-contacting face seals. They mentioned in their paper that even unplanned unevenness such as circumferential waviness or micro irregularities help to generate significant hydrodynamic pressure. It was also found that the shape of film gap has a very critical influence on film stability, stiffness and leakage rate.

Wu (1970) analyzed the behavior of the squeeze film between two annular disks. Murti (1974) found that increasing permeability decreases the squeeze film pressure. He has shown that when two plates approach each other, a portion of the fluid flows out through the porous facing and thus squeezing time is reduced. Also the pressure distribution becomes more uniform with considerable reduction in the peak pressure magnitude. Whereas, Ting (1975) and later Ahmad *et al.* (1998) studied the effect of permeability on the engagement behavior of lubricated porous annular disks. But neither the effect of the viscoelastic deformation of porous material nor roughness of the mating surfaces was considered. Actually, all these studies focus upon the squeeze-film performance with the ideal assumption that mating surfaces are perfectly smooth. However, engineering surfaces are generally rough due to the processes used in forming and finishing stages. On the other hand, the roughness height is usually of the same order as the mean asperity in a lubricated contact. Under these considerations, the influence of surface roughness on the squeeze film characteristics should be noted. Rohde *et al.* (1979), Hori and Kato (1979), Hori *et al.* (1981) and Yoo (1987) have demonstrated that in case of high frequency of squeezing motion, the viscoelastic effects of the solid on pressure generation in the fluid film can not be ignored. Lai (1980) and Snegovsky and Buljuk (1983) showed that macrocavities or grooves with small depth may also keep the parallel faces apart from each other. The squeeze film between porous mating surfaces of low elastic modulus materials have been investigated as an elastohydrodynamic (EHL)

3

problem by many such as Wada and Nishida (1985), Ikeuchi *et al.* (1989) and Horikawa *et al.* (1990).

Lin *et al.* (2002) have shown that the mean squeeze-film characteristics of a long partial journal bearing operating under a time-dependent oscillating load are significantly affected by the height and the pattern of roughness in both transverse and longitudinal directions. Kaneko *et al.* (2004) found that the effect of viscoelascity of porous rubber and fluid inertia on surface deformation cannot be ignored for the surfaces oscillating at or more than a frequency of 40 Hz. But they did not consider the effect of surface roughness of the mating surfaces and permeability of rubber material on side leakage flow and hydrodynamic force. Bujurke *et al.* (2006) have investigated the effect of surface roughness on the squeeze film characteristics of long porous partial journal bearings with couple stress fluids as lubricant. He found that couple stresses increase the load carrying capacity and the response time where as the permeability parameter decreases the load carrying capacity and decrease the response time as compared to the non-permeable case.

Surface roughness of porous rubber has significant effect on hydrodynamic load as well as on leakage flow especially for bearings, wet clutches and static seals under axial vibration. For the sake of two dimensional analysis, longitudinal roughness pattern as shown in Figure 1.1 is considered for the present work. Surface irregularities of porous rubber block can considerably decrease leakage flow rate with increasing hydrodynamic force which is much advantageous for many engineering applications. Deformation of porous rubber block during squeezing requires viscoelastic consideration. None of the above mentioned works provides a comprehensive model considering the combined effect of permeability, surface roughness and viscoelasticity. In the present research cavitation and thermal distortion of the rubber surface are ignored. Surface roughness of the rigid block is also not considered here.
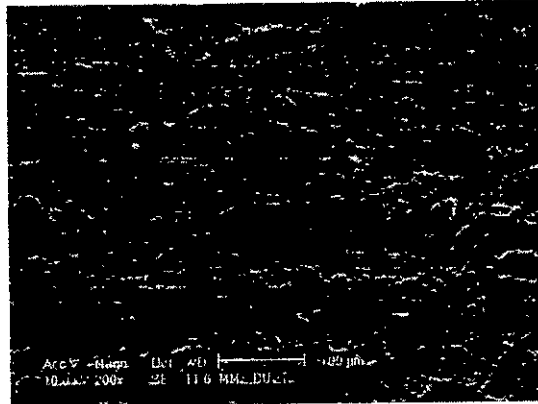
Figure 1.1 Images (200X) taken by Scanning Electron Microscope (SEM) of longitudinal roughness pattern. [Images are taken in SEM lab of MME Dept., BUET]

1.3 Objective of the Present Research

The specific objectives of the present research are as follows:

(a)　To develop a mathematical model for the prediction of performance of a squeeze film between a rubber surface and an oscillating rigid surface.

(b)　To conduct a parametric analysis using the developed model to investigate the effect of permeability and surface roughness of the porous rubber block as well as oscillating frequency of the rigid plate on hydrodynamic load and leakage flow.

A mathematical model is developed in such a way that a rigid block facing the porous rubber block is oscillating sinusoidally in the direction perpendicular to its surface. When the rigid block moves downward towards the porous block, it squeezes the lubricating oil film retaining between the clearance gap producing high positive pressure. While it moves upward producing huge negative pressure lubricating oil is

drawn into the clearance gap between the mating surfaces. The values of pressure in the fluid film as well as in the porous matrix and the surface deformation of the porous rubber block will be obtained by simultaneously solving the Reynolds equation, the Laplace equation and three-parameter viscoelastic model. Numerical methods applied to solve the equations are discussed in the next chapter.

1.4 Outline of the Thesis

This thesis consists of four chapters. The entire work is based on mathematical model and numerical simulation.

Chapter 1 gives the background of this research work and defines the purpose and directions of investigation.

In Chapter 2 a mathematical model is developed to simulate with a numerical approach such as finite difference methods. As the simulation results are satisfactorily validated by the available experimental data, the model is used for further investigation to obtain a good understanding of the squeeze film phenomena between a rigid surface and a porous rubber block.

Chapter 3 presents results and discussion obtained from numerical simulation.

In Chapter 4 outcome of the research work has been summarized.

Chapter 2

Mathematical Model

2.1 Introduction

Figure 2.1(a) shows a schematic diagram of the simple model investigated in the present study. A cylindrical porous rubber block whose bottom surface is attached to a rigid holder is used as a deformable permeable material and its upper surface faces a rigid plate. The porous block and the rigid plate are separated by a distance, h, and the rigid plate is oscillated sinusoidally in the direction perpendicular to its surface.

It is assumed that the clearance gap and the porous material are filled with lubricant oil, and the ambient pressure in the surrounding fluid (lubricant oil) is atmospheric pressure. Figure 2.1 (b) shows the coordinate system used in the analysis. Cylindrical coordinates are used for the axisymmetric model. For simplicity, the deformation (δ_s) of the porous rubber surface is transferred to the bottom surface of the rigid plate. The axial coordinate through the film thickness y is measured upward from the porous rubber surface. For the imposed squeezing motion of the rigid plate, the hydrodynamic pressure will be developed in the clearance gap and the porous material and will deform the rubber surface. Again due to this deformation, the pressure profile, in turn, will be modified, and so on. Thus the iteration continues until stable pressure profile and deformation is obtained.

It will be assumed that the porous rubber block has uniform porosity and permeability. Deformation of the cylindrical porous rubber block will be evaluated based on a three-element viscoelastic model.

Rigid plate

$v_h[=-2\pi f a_s \sin(2\pi f t)]$

Lubricant oil

$h[=h_0 + a_s\{\cos(2\pi f t)-1\}+\delta_s]$

Porous rubber block

r_a

L
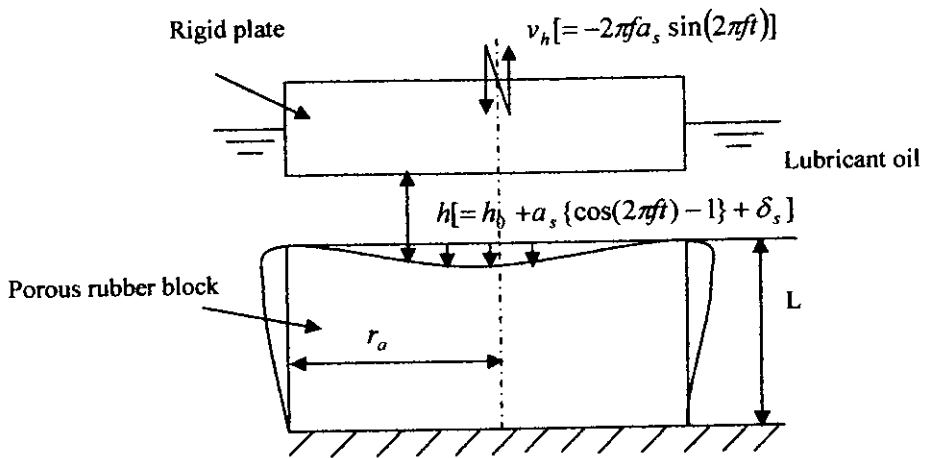
Figure 2.1 (a) Problem geometry

v_h

Lubricant Oil

h

y

Porous rubber block
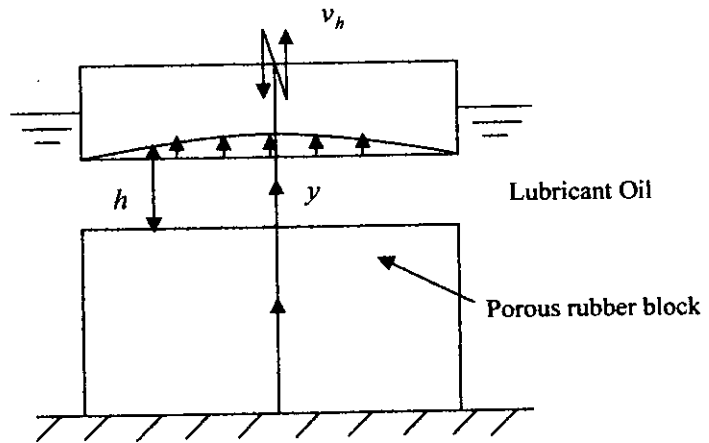
Figure 2.1 (b) Co-ordinate system

8

The pressures in the fluid film and the porous material and the surface deformation of the porous rubber block will be obtained by simultaneously solving the Reynolds equation, the Laplace equation and the three-parameter viscoelastic model. Equations will be discretized by finite difference scheme and then solved by Guass-Siedel Iteration method. Once the pressure and the deformation are determined, the performance parameters can be calculated.

2.2 Three-element Viscoelastic Model (Standard Linear Solid)

Some materials show a pronounced influence of the rate of loading, the strain being larger if the stress has grown more slowly to its final value. The same materials display creep, that is, an increasing deformation under sustained load, the rate of strain depending on the stress. Such materials are called viscoelastic. Among them are metals at elevated temperatures, concrete, plastics, polymers and polymer-matrix composites. While not all polymers are viscoelastic to any important practical extent, and even fewer are linearly viscoelastic, this theory provides a usable engineering approximation for many applications in polymer and composites engineering. For more typical polymers whose conformational change is eventually limited by the network of entanglements or other types of junction points, more elaborate spring-dashpot models can be used effectively. Placing a spring in series with a spring and a dashpot connected parallelly as shown in Figure 2.2 gives a very useful well known model as three element viscoelastic model. It is also known as the standard linear material. For the both strains of both parts, stresses can be expressed as

$$\sigma = E\varepsilon'$$

$$\sigma = q_0'' \varepsilon'' + q_1'' \overset{\bullet}{\varepsilon}{}''$$
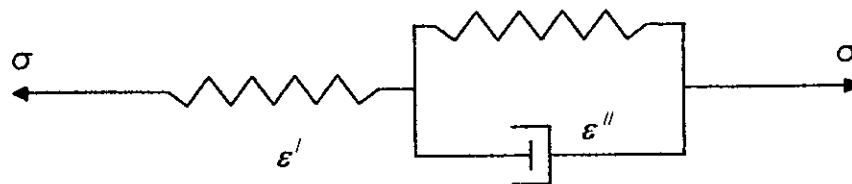
Figure 2.2 Three element viscoelastic model

9

The Laplace transformation is very convenient in this model because it reduces differential equations to algebraic ones. q_0'', q_1'' and E are the coefficients of the constitutive equation which are determined experimentally for specific materials.

2.3 Governing Equations for Fluid Film Pressure

The fluid is assumed to be an incompressible Newtonian substance with constant properties. The flow is also assumed axisymmetric ($\partial/\partial\theta = v_\theta = 0$). Applying the hydrodynamic lubrication assumption for thin films, and retaining both local and convective inertia terms, the equations of motion in r and y direction can be expressed, respectively, as

$$\rho(\frac{\partial v_r}{\partial t} + v_r\frac{\partial v_r}{\partial r} + v_y\frac{\partial v_r}{\partial y}) = -\frac{\partial p}{\partial r} + \eta\frac{\partial^2 v_r}{\partial y^2} \tag{1}$$

$$\frac{\partial p}{\partial y} = 0 \tag{2}$$

The continuity equation is,

$$\frac{1}{r}\frac{\partial}{\partial r}(rv_r) + \frac{\partial v_y}{\partial y} = 0 \tag{3}$$

Equation (2) states that the film pressure, p, is constant across the thickness of the film. This is based on the fact that the squeeze film is thin and thereby the pressure cannot vary significantly across it. On the other hand, the effect of tangential velocity slip at the interface between the fluid film and the porous rubber surface is relatively small. Hence, using the no-slip condition (Wu, 1970), the boundary conditions on v_r, v_y, and p are given as

$$\text{at} \qquad y = 0, \qquad v_r = 0, \qquad v_y = -\frac{k}{\eta}\frac{\partial p_m}{\partial z}\Big|_{z=L} \tag{4}$$

10

at $\quad y = h, \quad v_r = 0 \quad\quad v_y = \dot{h}$ $\hspace{3cm}$ (5)

at $\quad r = 0 \quad\quad \dfrac{\partial p}{\partial r} = 0$ $\hspace{3cm}$ (6)

at $\quad r = r_a \quad p = p_a(=0) \quad$ if $v_{rm} \geq 0 \quad$ & $\quad p = p_a - \delta p \quad$ if $v_{rm} < 0$ $\quad$ (7)

where p_m is the pressure in the porous material and $\dot{h}$ the squeezing velocity. Since the rigid plate is oscillated sinusoidally with frequency f, the film thickness will change as

$$h = h_0 + a_s\{\cos(2\pi f t) - 1\} + \delta_s \hspace{3cm} (8)$$

where h_0, a_s and δ_s are the initial film thickness, the amplitude of the rigid plate oscillation and the deformation of the porous rubber surface, respectively. In Eq. (5) $\dot{h}$ is thereby given as

$$\frac{dh}{dt} = \dot{h} = -2\pi f a_s \sin(2\pi f t) + \dot{\delta}_s \hspace{3cm} (9)$$

In Eq. (7), p_a stands for the ambient pressure, which is assumed to be equal to the atmospheric pressure. Equation (7) states that when the surrounding fluid enters the clearance gap, the fluid is accelerated radially and thereby the fluid pressure at $r = r_a$ becomes lower than the ambient pressure by an amount δp. This pressure drop δp can be expressed as,

$$\delta p = \rho(1 + \xi)v_{rm}^2 / 2 \hspace{3cm} (10)$$

where ξ denotes the inlet loss coefficient and is empirically given a value of 0 to 1.0 (Kaneko *et al.*, 2004). In the present analysis, a value of 0.5 is assumed for ξ. Moreover, v_{rm} is the radial velocity averaged across the film thickness at $r = r_a$, being described later on.

11

2.4 Governing Equations for Pressure in Porous Material

It is assumed that the porous rubber block has uniform porosity and permeability. This assumption is based on the fact that the maximum strain of the porous material due to the pressure in the squeeze film and the porous material is predicted to be 0.4% (Kaneko *et al.*, 2004) near the center of the porous rubber surface whereas the order of magnitude for the mean pore size is in the range 0.24 mm to 0.42 mm. This suggests that the local deformation of the porous material is much small compared to the pore size and thereby the quantitative effect of the strain on the local variations of the porosity and the permeability is not significant. Moreover, the fluid inertia effect due to the seepage velocity in the porous material is assumed to be negligibly small as the seepage velocity is much smaller than the fluid velocity in the squeeze film. By substituting the fluid velocity components obtained from Darcy's law into the continuity equation, the governing equation for the pressure p_m in the porous material is expressed as the following Laplace equation:

$$\frac{\partial}{\partial r}\left(r\frac{\partial p_m}{\partial r} \right) + r\frac{\partial^2 p_m}{\partial z^2} = 0 \qquad (11)$$

with the boundary condition

For solid rubber block, $r = 0$ $\qquad \dfrac{\partial p_m}{\partial r} = 0$ $\qquad\qquad (12)$

$\qquad\qquad\qquad\qquad r = r_a$ $\qquad p_m = p_a = 0$ $\qquad\qquad (13)$

$\qquad\qquad\qquad\qquad z = 0$ $\qquad \dfrac{\partial p_m}{\partial z} = 0$ $\qquad\qquad (14)$

$\qquad\qquad\qquad\qquad z = L$ $\qquad p_m = p$ $\qquad\qquad (15)$

2.5 Reynolds Equation

Substituting the Darcy's law and Eq. (11) into the Eqs. (1) and (3) and using the boundary conditions, the governing equation is obtained as follows:

$$\frac{\partial}{\partial r}\left(rh^3 \frac{\partial p}{\partial r}\right) = 12\eta r\left(\overset{\bullet}{h}+ \frac{k}{\eta}\frac{\partial p_m}{\partial z}\Big|_{z=L}\right) \qquad (16)$$

2.6 Deformation of Rubber Surface

In the present analysis, an axisymmetric viscoelastic continuum model is introduced for the porous rubber block and its constitutive equations will be derived as follows:

Here the rubber block is considered as a three-parameter solid and using the three parameter viscoelastic model the deformation of the rubber block is obtained. From Kelvin model and Maxwell model following equations can be deduced,

$$\sigma = E\varepsilon' \qquad \text{and} \qquad \sigma = q_0''\varepsilon'' + q_1'' \overset{\bullet}{\varepsilon}^{''} \qquad (17)$$

To both equations, the Lapalce transformation is applied on both sides. Since E, q_0'' and q_1'' are constants, this yields

$$\overline{\sigma} = E\overline{\varepsilon'}, \qquad \overline{\sigma} = (q_0'' + sq_1'')\overline{\varepsilon''} \qquad (18)$$

Multiplying each of Eq. 18 with a suitable constant and adding, it is found,

$$\overline{\sigma}\left(q_0'' + sq_1''\right)+ E\overline{\sigma} = E\left(q_0'' + sq_1''\right)\left(\overline{\varepsilon'}+ \overline{\varepsilon''}\right) = E(q_0'' + sq_1'')\overline{\varepsilon} \qquad (19)$$

where $\overline{\varepsilon}$ is the transform of the total strain. Transforming back into the physical plane means removing bars and replacing every factor s by a differentiation:

$$(q_0^{//} + E)\sigma + q_1^{//}\,\dot{\sigma} = Eq_0^{//}\varepsilon + Eq_1^{//}\,\dot{\varepsilon} \tag{20}$$

Eq. (20) is written in the normalized form as follows:

$$\sigma + p_1\,\dot{\sigma} = q_0\varepsilon + q_1\,\dot{\varepsilon} \tag{21}$$

Comparing the coefficients of both equations Eq. (20) & Eq. (21) it can be found that

$$p_1 = \frac{q_1^{//}}{(E + q_0^{//})} \tag{22}$$

$$q_0 = \frac{Eq_0^{//}}{(E + q_0^{//})} \tag{23}$$

$$q_1 = \frac{Eq_1^{//}}{(E + q_0^{//})} \tag{24}$$

and from Eq. (22), (23) & (24) it follows that

$$\frac{q_1}{p_1} - q_0 = \frac{E^2}{E + q_0^{//}} \tag{25}$$

Condition arises from the Eq. (25) that right hand side term is always positive if

$$q_1 > p_1 q_0$$

In the creep phase it follows

$$\sigma = \sigma_0 \Delta(t), \qquad \overline{\sigma} = \frac{\sigma_0}{s}$$

From the Laplace transform of Eq. (21) it follows

14

$$\sigma_0 \left(\frac{1}{s} + p_1 \right) = (q_0 + q_1 s)\bar{\varepsilon}$$

where σ_0 is initial stress applied to the viscoelastic material

$$\Rightarrow \bar{\varepsilon} = \sigma_0 \frac{1 + p_1 s}{s(q_0 + q_1 s)} = \frac{\sigma_0}{q_1} \left[\frac{1}{s(s + \lambda)} + \frac{p_1}{s + \lambda} \right] \quad (26)$$

with $\lambda = \dfrac{q_0}{q_1}$ doing Inverse Laplace transformation of Eq. (26) strain is obtained as

$$\varepsilon = \frac{\sigma_0}{q_1} \left[\frac{1}{\lambda}(1 - e^{-\lambda t}) + p_1 e^{-\lambda t} \right] \quad (27)$$

since $\sigma_0 = P_T$ Eq. (27) may be written as

$$\varepsilon = \frac{P_T}{q_0} \left[1 - (1 - \frac{p_1 q_0}{q_1})e^{-\frac{q_0 t}{q_1}} \right] \quad (28)$$

where P_T is the pressure generated in fluid film and in the porous material.

Coefficients of the constitutive equations for one-dimensional viscoelastic model are obtained from the experimental data by Kaneko et al. (2004) as follows:

Table 2.1: Coefficients of the constitutive equations

Coefficients	Values	Unit
p_1	2.48E-3	Sec
q_0	6.08	MPa
q_1	27.7856	kPa-s

2.7 Rough Surface Generation

Two dimensional rough surfaces can be generated by producing random variables. Codes are written in MATLAB to generate random variables as follows:

$$x = m + \text{sqrt}\ (\mu^2)\ *\ \text{randn}\ (r,c)$$

m = arithmetic mean

r= row and c=column

The **randn** function generates arrays of random numbers using Ziggurat method under symmetrical Gaussian distribution whose elements are normally distributed with mean 0, variance $\mu^2 = 1$, and standard deviation $\mu = 1$. To generate a random distribution with a specific mean and variance, first step is to multiply the output of randn by the standard deviation and then add the desired mean. Two main parameters for describing rough surface are involved in this code. Symmetrical Gaussian rough surface is generated by varying one parameter keeping constant of other parameter. As arithmetic mean and standard deviation both are height function these are not enough for describing rough surface precisely. So autocorrelation function and autocorrelation length is calculated by the following formula:

$$C(\tau) = \lim_{L=\infty} \int_0^L [z(x) - m][z(x+\tau) - m]dx = \left[R(\tau) - m^2\right]/\mu^2 \qquad (29)$$

Where as m = arithmetic mean and $z(x)$ is the height function of the surface (as described in Appendix A.4.2).

2.8 Hydrodynamic Force

In the present model, local hydrodynamic pressures are computed numerically at various grid points over the rubber surface and hydrodynamic force F is obtained by the following equation:

$$F = 2\pi \int prdr \qquad (30)$$

2.9 Leakage Flow Rate

The radial leakage flow from the film region through the clearance gap (Q_r) is expressed with the axial leakage flow from the clearance gap into the porous material (Q_p) and the variation in volume of the clearance gap with time $(\dot{V})$ considering smooth surface of the rubber block as,

$$Q_r = -\dot{V} - Q_p \tag{31}$$

where

$$\dot{V} = 2\pi \int_0^{r_a} \dot{h} r \, dr \tag{32}$$

$$Q_p = 2\pi \int_0^{r_a} \frac{k}{\eta} \left(\frac{\partial p_m}{\partial z} \bigg|_{z=L} \right) r \, dr \tag{33}$$

$$Q_r = 2\pi r_a \, \bar{h} . v_{rm} \tag{34}$$

Substituting Eqs. (31)- (33) into Eq. (30) gives,

$$v_{rm} = -\frac{1}{r_a \bar{h}} \int_0^{r_a} \left(\dot{h} + \frac{k}{\eta} \frac{\partial p_m}{\partial z} \bigg|_{z=L} \right) r \, dr \tag{35}$$

v_{rm} is the average velocity in radial direction considering smooth surface. If surface of the rubber block is considered as rough surface, average clearance gap becomes less and leakage flow rate along the radial direction reduces. At minimum seal clearance leakage flow rate becomes minimum. Flow rate is calculated considering roughness of the rubber surface as follows:

$$Q = 2\pi r_i h_{n.clearance} v_{rm} \tag{36}$$

Average seal clearance $h_{a.clearance}$ depends on the height distribution of the asperities over the rubber surface. Height distribution of the asperities can be conveniently expressed as center line average (CLA) and standard deviation μ. With increasing CLA the average

clearance for fluid film decreases. Therefore average seal clearance is expressed as follows:

$$h_{n.clearance} = (\bar{h} - \mu) \tag{37}$$

where $h_{n.clearance}$ denotes net clearance for fluid between the mating surfaces, $\bar{h}$ is arithmetic mean of film thickness and μ is standard deviation of the surface height of rubber block.

2.10 Numerical Solution

The application of finite differences is commonly found in the numerical solution to elliptic partial differential equations such as a Laplacian, $\nabla^2 f = 0$ or a Poisson's equation, $\nabla^2 f = g(x, z)$. Finite difference method is preferable to finite element method because of the advantages of less computational time and simplified model.

2.10.1 Finite Difference Equations

Discretized Reynolds equation: fluid film pressure

The hydrodynamic pressure distribution within lubricated face seal interface can be determined from the numerical solution of the Reynolds equation. The numerical analysis starts with the following modified Reynolds equation including the pressure term in the porous media

$$\frac{\partial}{\partial r}\left(rh^3 \frac{\partial p}{\partial r} \right) = 12\eta r \left(\dot{h} + \frac{k}{\eta}\frac{\partial p_m}{\partial z}\Big|_{z=L} \right)$$

This equation can be discretized as follows,

$$\frac{1}{4(\Delta r)^2}\left\{(r_{i,j+1}h_{i,j+1}^3)(3P_{i,j+1}-4P_{i,j}+P_{i,j-1})+(r_{i,j-1}h_{i,j-1}^3)(3P_{i,j-1}-4P_{i,j}+P_{i,j+1})\right\}$$

$$=12\eta r_{i,j}\overset{\bullet}{h}_{i,j}+12r_{i,j}k\frac{(3P_{mi,j}-4P_{mi-1,j}+P_{mi-2,j})}{2(\Delta z)}$$

This equation can be simplified as follows:

$$(r_{i,j+1}h_{i,j+1}^3)(3P_{i,j+1}-4P_{i,j}+P_{i,j-1})+(r_{i,j-1}h_{i,j-1}^3)(3P_{i,j-1}-4P_{i,j}+P_{i,j+1})$$

$$=\left[4\times12\eta(\Delta r)^2\right]r_{i,j}\overset{\bullet}{h}_{i,j}+\left[\frac{4\times12(\Delta r)^2 k}{2(\Delta z)}\right]r_{i,j}(3P_{mi,j}-4P_{mi-1,j}+P_{mi-2,j})$$

$$\Rightarrow (R_j H_{j+1}^3)(3P_{i,j+1}-4P_{i,j}+P_{i,j-1})+(R_{j-1}H_{j-1}^3)(3P_{i,j-1}-4P_{i,j}+P_{i,j+1})$$

$$=C_1 R_j \overset{\bullet}{H}_j+C_2 R_j(3P_{mi,j}-4P_{mi-1,j}+P_{mi-2,j})$$

(38)

where

$$r_{i,j}=R_j \text{ and } h_{i,j}=H_j$$

$$C_1=\left[48\eta(\Delta r)^2\right]$$

$$C_2=\left[24\frac{(\Delta r)^2}{(\Delta z)}k\right]$$ where k is intrinsic permeability and η is dynamic viscosity and

$$H_j=h_0+a_s\left\{\cos(2\pi ft)-1\right\}+\frac{P_{Tj}L}{q_0}[1-(1-\frac{p_1 q_0}{q_1})e^{-\frac{q_0 t}{q_1}}]$$ (From Viscoelastic model)

Discretized boundary condition may be written as,

At $r = 0$ the discretized equation is $-P_{i,j+2} + 4P_{i,j+1} - 3P_{i,j} = 0$

And at $r = r_a$ the equation is $P = 0$ & $P = -\rho(1+\xi)\dfrac{v_{rm}^2}{2}$ depending on the direction of

v_{rm}

Laplace equation: pressure in porous material

The governing equation for pressure P_m in the porous material is expressed as the Laplace equation. Finite difference form of the Laplace equation can be written as follows:

$$(1+\frac{\Delta r}{2R_j})P_{mi,j+1} + (1-\frac{\Delta r}{2R_j})P_{mi,j-1} - 2\{1+\left(\frac{\Delta r}{\Delta z}\right)^2\}P_{mi,j} + \left(\frac{\Delta r}{\Delta z}\right)^2 P_{mi+1,j} + \left(\frac{\Delta r}{\Delta z}\right)^2 P_{mi-1,j} = 0$$

(39)

Finite difference equations for boundary conditions are as follows:

At $z = 0$ $-P_{mi+2,j} + 4P_{mi+1,j} - 3P_{mi,j} = 0$

At $r = 0$ $-P_{mi,j+2} + 4P_{mi,j+1} - 3P_{mi,j} = 0$

At $r = r_a$ $P_{mi,j} = 0$ and at $z = L$ $P_{mi,j} = P_{i,j}$

Discretized equation for leakage flow rate

Leakage flow rate can be determined form the Eq. (35). Integral equation is involved in the term radial velocity v_{rm} as shown in Eq. (34). Trapezoidal rule is applied for solving Eq.(34) to evaluate the radial velocity. Equation (34) can be discretized as follows:

$$v_{rm} = -\frac{f_{i,0} + 2\sum_{j=1}^{seg-1} f_{i,j} + f_{i,seg}}{2segR\bar{h}} \qquad (40)$$

where $f_{i,j} = \left[\dot{H}_j + \frac{k}{2\eta\Delta z}\left(-P_{mi+2,j} + 4P_{mi+1,j} - 3P_{mi,j}\right)\right]R_j$ and seg = number of segment

The pressure in the fluid film and porous material can be obtained by solving Eq. (37) and (38) simultaneously by Gauss-Siedel Iteration Method. Cylindrical porous rubber block is considered as axisymetric. In order to calculate the pressure in the porous material the cylindrical porous rubber block is divided into 48 nodes along the radial direction and 16 nodes along the z-direction. In order to calculate fluid film pressure, region of fluid film between the mating surfaces is also divided into 48 nodes along the radial direction. Therefore, fluid film pressure is obtained solving Eq. (37) taking 48×48 nodal points. At each time step, the iteration is continued until the following condition is satisfied:

$$\frac{\sum_{i,j}\left|p_{i,j}^{(n+1)} - p_{i,j}^{(n)}\right|}{\sum_{i,j} p_{i,j}^{(n)}} < 10^{-5} \qquad (41)$$

$$\frac{\sum_{i,j}\left|\delta_{si,j}^{(n+1)} - \delta_{si,j}^{(n)}\right|}{\sum_{i,j} \delta_{si,j}^{(n)}} < 10^{-3} \qquad (42)$$

In Eq. (39) n and $n+1$ denote two consecutive iterations, $p_{i,j}$ is the nodal pressure at point (i,j) in which i and j represent the grid number in radial and axial directions respectively.

2.11 Solution Procedure

The pressures in the fluid film and the porous material and the surface deformation of the porous rubber block will be obtained by simultaneously solving the Reynolds equation, the Laplace equation and the three-parameter viscoelastic model.

21

At first, a value of fluid film pressure and a value of film thickness between the mating surfaces are arbitrarily assumed at time $t = 0$ for initialization of the solution procedure. This assumed value of fluid film pressure is considered as boundary condition for solving Laplace equation (Eq. 11) to evaluate pressure rise in the porous material. Laplace equation is discretized into finite difference equation. Porous rubber block is divided into a finite number of nodes. Finite difference equation is applied to each node in the porous rubber block. A diagonal matrix will be formed and solved by Gauss-Siedel iteration to evaluate pressure in the porous material.

Viscoelastic deformation of rubber surface will occur due to fluid film pressure and pressure developed in the porous material. This deformation of rubber surface is calculated by solving Eq. (28). When rubber surface is deformed film thickness will be changed (Eq. 8). New film thickness will replace assumed initial film thickness. This new film thickness will be used in Reynolds equation.

Reynolds equation (Eq. 16) is also discretized into finite difference equation. Fluid film region is divided into a finite number of nodes. Finite difference equation is applied to each node in fluid film region. Again, a diagonal matrix will be formed and solved by Gauss-Siedel iteration to evaluate fluid film pressure.

Updated fluid film pressure and viscoelastic deformation of rubber surface are checked for convergence by comparing with previous film pressure and viscoelastic deformation. Stopping criteria of iteration is set by Eqs. (40) & (41). If Eqs. (40) & (41) are satisfied, further iteration will be stopped. Finally, profile of fluid film pressure and viscoelastic deformation of rubber surface will be found. Otherwise calculated film pressure and viscoelastic deformation will be used for further iteration and same procedure will be followed. Thus the iteration continues until stable pressure profile and deformation is obtained. A complete flow chart of solution procedure is given as follows:
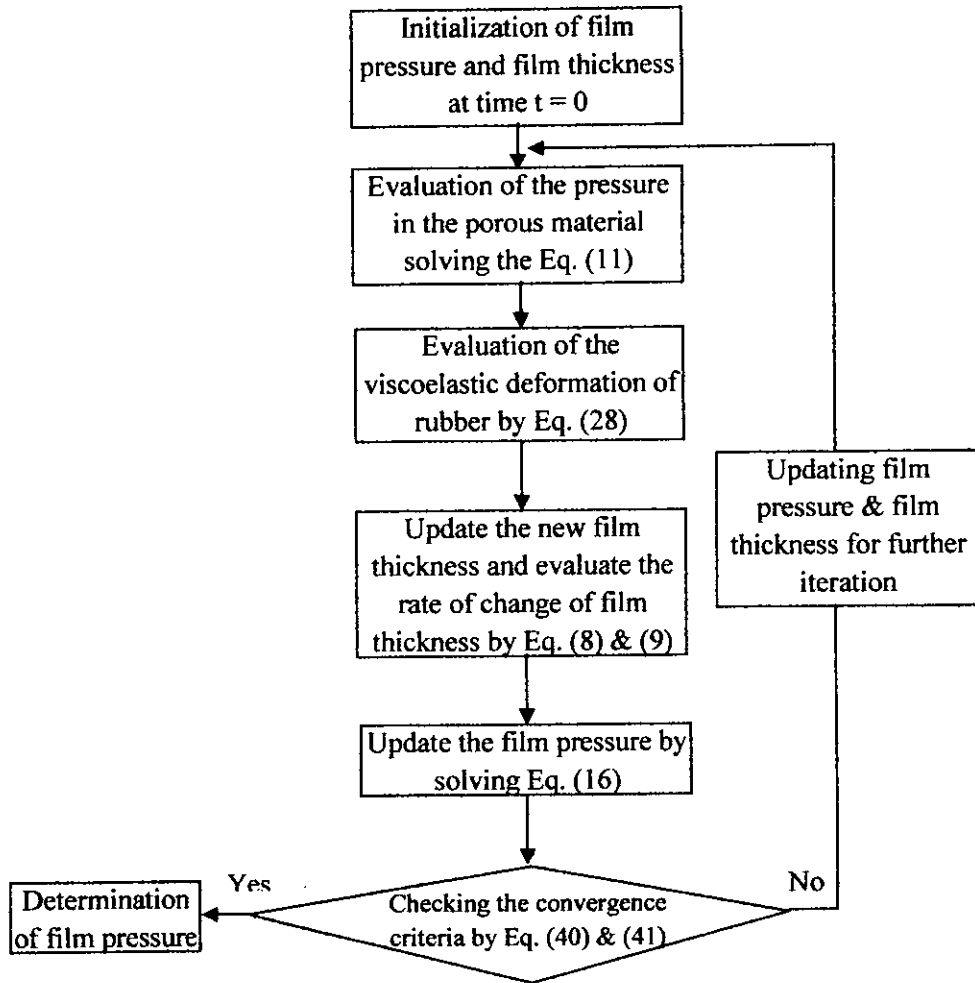
Figure 2.3 Flow chart for solution procedure

2.12 Grid Dependency Test

To investigate the influence of number of nodal points in the radial and axial directions of porous rubber block 40×40, 48×48 and 54×54 were used as trial. The Figure 2.4 reveals the variation of hydrodynamic force (F) developed in the fluid film between the mating surfaces with dimensionless time parameter (T). Dimensionless time parameter is calculated with respect to oscillating frequency (f) and absolute time (t). The results

presented in Figure 2.4 show that the difference between the squeeze film characteristics obtained by mesh size of 48×48 and 54×54 is quite small. This suggests that mesh sizes of 48×48 are sufficient to correctly evaluate the squeeze film characteristics. Squeeze Reynolds number Re_s is evaluated to be 0.221 for $f = 10$ Hz and 0.443 for $f = 20$ Hz.
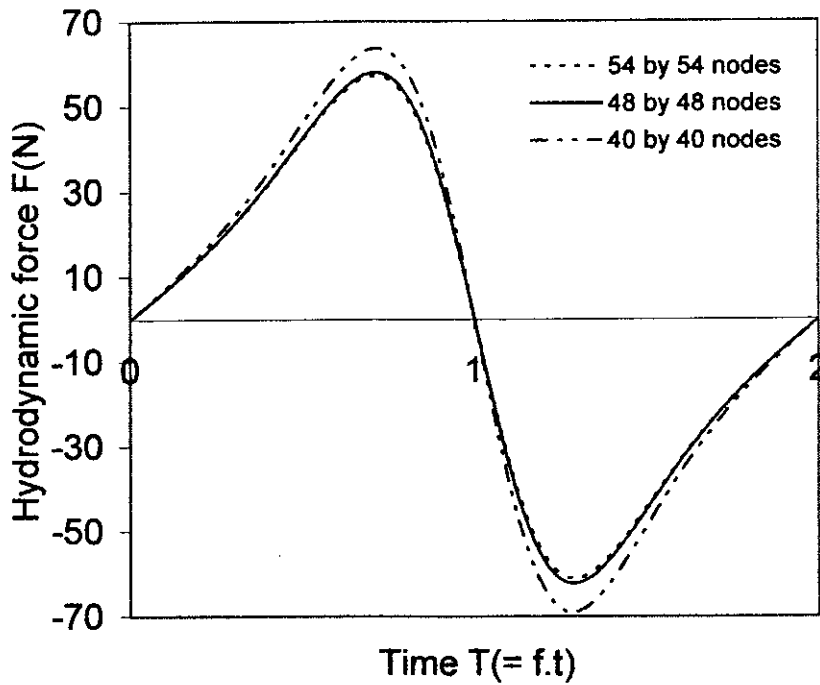
Figure 2.4 Grid dependency test considering variation of hydrodynamic film force varied with time for the frequency 10 Hz for various numbers of nodes.

Chapter 3

Results and Discussion

3.1 Introduction

Hydrodynamic pressure developed in the fluid film between the rubber surface and rigid surface is computed using the numerical scheme as described in the previous chapter. Hydrodynamic force is generated in this fluid film between the mating surfaces during squeezing motion. Leakage flow indicates the fluid flow from clearance between the mating surfaces to the surroundings along the radial direction. In this chapter, effects of various roughness parameters and permeability of porous rubber block on hydrodynamic force and leakage flow rate will be discussed. For the validation of numerical code, results obtained from proposed model are also compared with previous numerical and experimental results available in the literature.

For computation different input parameters are used which are shown in Table 3.1

Table 3.1: Different input parameters

Name of the parameters	Symbol	Numerical values	Unit
Diameter of rubber block	D	98	mm
Thickness of rubber block	L	29.2	mm
Permeability of rubber	k	2.63×10^{-10}	m^2
Porosity	-	35.7	%
Absolute viscosity	η	0.116	Pa.s
Density	ρ	970	kg/m^3
Temperature	-	20	^0C
Amplitude of oscillation	a_s	0.3	mm
Initial film thickness	h_0	1.4	mm
Minimum film thickness	h_{min}	1.1	mm

In the present work, oscillating squeeze film between the mating surfaces is modeled with silicone oil operated at atmospheric pressure. Fluid film between two mating surfaces shows different hydrodynamic behavior depending on film thickness. Therefore, according to film thickness, fluid film is divided into five regimes. These regimes can be shown in the familiar Stribeck curve in Figure 3.1 (Stribeck, 1902). The regimes of lubrication are sometimes identified by a lubricant film parameter equal to h_{min}/μ. In the present work, it is assumed that fluid film is operated in the hydrodynamic regime and no solid-solid contact occurs between the mating surfaces. From the figure 3.1 it is found that to operate fluid film in hydrodynamic regime minimum clearance must be kept at $h_{min}/\mu \geq 3.92$. A computer program is developed so that if the value of h_{min}/μ goes below 3.92, further iteration will be stopped. It is also assumed arbitrarily that the rigid block is oscillating over the rubber block at a finite amplitude of 0.3 mm.

3.2 Validation of the Numerical Code

Hydrodynamic pressure developed in the fluid film between the rubber block and the rigid surface is computed using modified Reynolds equation [Appendix B]. According to the characteristics of Reynolds equation, this film pressure denotes integral pressure throughout the fluid film. In the Figures 3.2 and 3.3, fluid film pressure vs. time curves are plotted. In the figures, along the x-axis time is plotted as dimensional parameter in terms of absolute time and oscillating frequency of rigid surface. The Figures 3.2 and 3.3 show the variation of hydrodynamic pressure developed in the fluid film between the mating surfaces at the center of rubber block with time. For the analysis, it is convenient to consider dimensionless time parameter which depends on oscillating frequency as well as absolute time. It is seen that the hydrodynamic pressure varies almost sinusoidally due to the oscillating motion of rigid block over the rubber block. A deformed shape of sinusoidal curve is found specially during increasing hydrodynamic pressure to the positive peaks in the Figures 3.2 and 3.3. It is because that squeeze time is more during squeezing period

than that of relaxation period. Therefore, hydrodynamic pressure increases slowly to the positive peaks than to the negative peaks. For the validation of numerical code, comparisons among results obtained from proposed model, previous Kaneko *et al.*'s (2004) model and experiment by Kaneko *et al.* (2004) are also shown in Figures 3.2 and 3.3.

The characteristic data on the porous rubber block, the lubricant oil and the coefficients in the constitutive equation employed in the numerical analysis are the same as those used in the experiment by the Kaneko *et al.* (2004). Good agreement is found comparing results obtained from the proposed model, Kaneko *et al.*'s model and experiment by Kaneko *et al.* for the frequency of oscillation 20 Hz and 10 Hz. The qualitative agreement of present results with experimental results implies the validity of the present numerical simulation.

The variation of hydrodynamic film force with time during sinusoidal oscillation of the rigid block is illustrated in Figure 3.4. In this figure comparison between the present result and the numerical result of Kaneko *et al.* for 20 Hz is also shown. Again, a good agreement of results is found between the present proposed model and the Kaneko's model. Figure 3.4 shows that the peaks of the hydrodynamic force become large as the frequency of the sinusoidal motion increases. Oscillating motion of rigid surface may be induced from engine vibration. Even after using dampers to dampen the vibration, often the frequency of vibration cannot be reduced to the zero value. But the advantageous fact is that with increasing frequency of oscillation the hydrodynamic force also increases as shown in Figure 3.4. This phenomenon helps to keep the mating surfaces apart maintaining proper oil film thickness in the clearance. This phenomenon is favorable in case of bearings, snow tires and wet clutches as high hydrodynamic force contributes to good load carrying capacity. High hydrodynamic force is also advantageous for non-contacting face seals because it keeps the mating surfaces apart maintaining proper oil film in the clearance. However, in case of non-contacting seals, optimization is necessary as leakage flow rate also increases with increasing frequency of oscillation.

As described in Chapter 2, three-parameter viscoelastic model is used in the present model to evaluate viscoelastic deformation at the center of the rubber block. In Figure 3.5 viscoelastic deformation is plotted against time for various permeability of porous rubber block. It is seen from the figure that viscoelastic deformation of rubber surface at the center of rubber block varies almost sinusoidally with time. Positive sign of deformation indicates compression occurring in the rubber block due to hydrodynamic force developed in the fluid film during squeezing period whereas negative sign of deformation indicates the opposite phenomenon. Negative value of viscoelastic deformation occurs due to the effect of viscoelasticity of rubber material. Deformed shape of oscillating curve of viscoelastic deformation is found as during compression more time is needed to raise hydrodynamic pressure to the peak value. Therefore, viscoelastic deformation of rubber surface at the center also increases slowly to the positive peak than to the negative peak. It is also seen that viscoelastic deformation decreases with increasing permeability of the porous rubber. It is because that with increasing permeability of the rubber block hydrodynamic force developed in the fluid film decreases which causes lower deformation of rubber surface. For the validation of three parameter viscoelastic model used in present model, result of viscoelastic deformation of rubber surface obtained from present model is compared with the result obtained from Kaneko *et al.*'s model and found a good agreement.

3.3 Application of the Model

The present model is applied to both solid and annular rubber blocks for the analysis of oscillating squeeze film between the rubber surface and the rigid surface. Effects of permeability and surface roughness of the rubber block on hydrodynamic force developed in the fluid film and leakage flow rate for the both cases are discussed here.

3.3.1 Case 1: Solid Rubber Block

Considering solid rubber block in the present model, it is assumed that a rigid surface is oscillating over a solid rubber block maintaining a fluid film in the clearance between the mating surfaces. Effects of surface roughness and permeability of the solid rubber block on hydrodynamic force and leakage flow rate will be discussed in this section.

3.3.1.1 Effect of the Surface Roughness

Center Line Average (CLA)

In the previous study (Kaneko *et al.*, 2004), analysis on the squeeze film between the oscillating rigid surface and the porous rubber surface was carried out without considering surface roughness of the rubber block. Practically, during the manufacturing processes like press forming process for rubber production surface roughness is generated on the rubber surface which has a significant effect on the hydrodynamic film force as well as leakage flow rate. Actually based on the theory of random processes, random and isotropic rough surface [Appendix A.3] can be completely characterized in a statistical sense by two functions: the height distribution and the spatial distribution. Height distribution of rough surface can be described by center line average (CLA) and standard deviation of the height of surface profile. Center line average (CLA) is the arithmetic mean of the absolute values of vertical deviation from the mean line through the surface profile as shown in Figure 3.6.

In the present work, CLA of surface height is calculated with the help of MATLAB code which is discussed in the previous chapter using following formula

$$CLA = \frac{1}{L} \int_0^L |z - m| dx \quad \text{and} \quad m = \frac{1}{L} \int_0^L z \, dx$$

where L is the sampling length.

Hydrodynamic force vs. time curve is plotted in Figures 3.7 and 3.8 under various center line average (CLA) of surface height for different frequencies of oscillation. It is found that due to sinusoidal oscillation of the rigid surface over the rubber block hydrodynamic force is developed in the fluid film between the mating surfaces. This hydrodynamic force also varies almost sinusoidally with time. Deformed shape of sinusoidal curve is found in the Figures 3.7 and 3.8 hydrodynamic force developed in fluid film increases slowly to the positive peak during squeezing period than to the negative peak during relaxation period. Positive hydrodynamic force is developed in the fluid film during squeezing and negative hydrodynamic force is developed when mating surfaces go apart. The figure also reveals that with increasing CLA values of surface height, hydrodynamic force increases significantly.

Similarly, Figures 3.9 & 3.10 show the variation of leakage flow rate with time under various center line average (CLA) of surface height of rubber block for the frequency 20 Hz and 10 Hz respectively. It is seen that leakage flow rate also varies sinusoidally with time due to oscillating motion of rigid surface over the rubber block. Positive flow rate indicates fluid flow towards surroundings from the clearance between the mating surfaces where as negative flow rate indicates the opposite phenomenon. It is also found that leakage flow rate decreases with the increasing CLA of surface height due to low clearance between the mating surfaces. When two mating surfaces move towards each other in normal direction, fluids need finite time to squeeze out through the clearance gap. Often fluids experience huge resistance to extrude through the gap between the mating surfaces. Due to low clearance this extrusion process is interrupted and some amount of fluid retains in the clearance gap.

Figure 3.11 shows the variation of maximum leakage flow rate and maximum hydrodynamic force with center line average (CLA) of surface height of rubber block. From the figure it is observed that increasing CLA of surface height of rubber block from 0 to 0.3 mm leakage flow rate decreases to 14% for 10 Hz and 19% for 20 Hz. It is because that minimum clearance between the mating surfaces decreases with increasing CLA of surface height that is illustrated in Figure 3.12. Figure 3.12

30

elucidates the variation of minimum clearance (h_{min}/μ) with CLA of the surface height of rubber block. From the figure it is seen that minimum clearance decreases proportionally with increasing CLA of surface height. Therefore, higher CLA of surface height of rubber block causes lower clearance between the mating surfaces. Due to low clearance fluid experiences more restrictions to squeeze out from the gap between the mating surfaces in the finite time period. From the Figure 3.11 it is clear that leakage flow rate decreases at higher rate for higher frequency. This phenomenon is suitable for non-contacting mechanical face seals. Low leakage flow rate also help to maintain proper film thickness in the clearance to avoid contacts between the mating surfaces. Again, as fluid gets less clearance to squeeze out, it experiences more resistance to extrude through the clearance resulting in huge hydrodynamic force. Figure 3.11 shows that with the increasing CLA of surface height from 0 mm to 0.3 mm, hydrodynamic force increases about 1.5 times for 10 Hz and 2 times for 20 Hz. High hydrodynamic force is often advantageous for bearing and wet clutch operation due to high load carrying capacity. Deformation of rubber surface occurs due to generating hydrodynamic force in the fluid film between mating surfaces. This deformation also contributes to avoid the contacts between the asperities of mating surfaces.

Standard Deviation (μ)

Standard deviation is also another important descriptor of height distribution of two dimensional surface roughness. Therefore, it is also important to analyze the effect of standard deviation of surface height of rubber block on hydrodynamic force and leakage flow rate. Standard deviation is a statistical term which denotes the mean deviation from the center line as shown in Figure 3.6. As described in the previous chapter, in the present work standard deviation of surface height of rubber block is calculated with the help of MATLAB code using following formula:

$$\mu = \sqrt{\frac{1}{L}\int_0^L (z-m)^2 dx} \quad \text{and} \quad m = \frac{1}{L}\int_0^L z\,dx \quad \text{where } L \text{ is the sampling length}$$

Figures 3.13, 3.14 & 3.15 show the variation of hydrodynamic force time under various standard deviation of surface height for the frequency 20 Hz, 15 Hz and 10 Hz respectively. In these figures it is seen that hydrodynamic force varies almost sinusoidally with time. Positive hydrodynamic force is developed in the fluid film during squeezing motion and negative hydrodynamic force is developed when mating surfaces go apart. It is also seen that hydrodynamic force increases significantly with increasing standard deviation of surface height of rubber block.

Variation of leakage flow rate with time under various standard deviation of surface height of rubber block for the frequency 20 Hz and 10 Hz is presented in Figures 3.16 and 3.17. It is observed that due to oscillation of rigid surface over the rubber block, leakage flow rate also varies sinusoidally with time. Leakage flow rate decreases with increasing standard deviation as higher standard deviation of the surface height causes more restrictions for fluid to squeeze out and huge hydrodynamic force is developed in fluid film.

Typical variation of maximum hydrodynamic force and maximum leakage flow rate with standard deviation of surface height of the rubber block is shown in the Figure 3.18. The figure shows the variation of hydrodynamic force and leakage flow rate with standard deviation of rubber surface under constant CLA and autocorrelation length. The figure reveals that with the increasing standard deviation of surface height of rubber block, leakage flow rate decreases. The reason is that fluid tends to stick in the valleys of rough surface. These valleys act as a reservoir for fluid and are responsible for decreasing leakage flow rate. Obviously it is seen that with increasing standard deviation of surface height of rubber block, hydrodynamic force increases as high standard deviation of the surface height of the rubber block causes more restrictions for fluid to squeeze out. Fluid faces high resistance for extrusion through the clearance between the mating surfaces and generates more hydrodynamic force. It is seen in the Figure 3.18 that hydrodynamic force increases about 36% as standard deviation increases from 0.0062 mm to 0.47 mm where as leakage flow rate decreases

3.3.1.2 Effect of Permeability

Advantage of using rubber materials in many engineering applications is not only to isolate vibration but also to reduce temperature rise in the mating surfaces by allowing penetration of the lubricating oil in the porous rubber material. Therefore, for optimum design, effect of permeability on leakage flow rate and hydrodynamic force is needed to study.

Permeability is a measure of the ability of a material to transmit fluids through the porous media. It is a property of the porous media only, not the fluid. It is cuased from the porosity and the definite pore size of the materials. Porosity is a measure of the void spaces in a material and is measured as a fraction between 0–1 or as a percentage between 0–100%. Numerical investigation is conducted by varying permeability from 2.63×10^{-10} m^2 to 2.63×10^{-09} m^2 and porosity form 35% to 55% (Appendix A.7).

In Figures 3.22-3.24 variation of hydrodynamic force with time under various frequency of oscillation is shown. Similarly leakage flow rate vs. time curves are presented in Figures 3.25-3.27. The Figures 3.22-3.24 reveal that with increasing permeability of porous rubber block hydrodynamic force decreases. This phenomenon can be of particular interest for bearing and wet clutch designers as highly permeable rubber material is not suitable to use in bearing or wet clutch applications due to low load carrying capacity. On the other hand Figures 3.25-3.27 illustrate that with increasing permeability leakage flow rate along the radial direction decreases slightly.

Clear idea may be found from Figure 3.28 which shows the variation of maximum hydrodynamic film force and maximum leakage flow rate with permeability of rubber block. It is observed from the figure that if permeability is increased by 10 times from 2.63×10^{-10} m^2, hydrodynamic force reduces to 17% but only 5% of leakage flow rate decreases for the frequency 15 Hz. Where as for 25 Hz, hydrodynamic force decreases to 25% and leakage flow rate decreases to 6.6%. Therefore, it can be

34

inferred that hydrodynamic force decreases at higher rate with increasing frequency of oscillation. This phenomenon is often unfavorable for design of bearing as the frequency of engine vibration may be increased several times which may reduce load carrying capacity. Therefore, optimization of permeability of rubber block is needed for bearing design. As permeability of rubber block has no significant effect on leakage flow rate, it is not of that much importance in case of seal design.

3.3.2 Case 2: Annular Rubber Block

In practical engineering applications, annular rubber block is used as thrust bearing pad and also in mechanical face seals. Effect of surface roughness on hydrodynamic force developed in fluid film between the mating surfaces and leakage flow rate will be discussed in this section considering annular rubber block. Leakage flow rate indicates the fluid flow through the outer clearance between the mating surfaces along the radial direction. Two annular rubber blocks available in local market are taken for the investigation. It is assumed that oscillating motion is induced to fluid film from engine vibration. Minimum clearance is limited up to $h_{min}/\mu \geq 3.92$ to operate fluid film in hydrodynamic regime. Iteration will be stopped if the value of minimum clearance goes below 3.92. Amplitude of the vibration is chosen arbitrarily at constant value of 10 micron. Different input parameters that are used in the model are shown in the table 3.2.

Table 3.2: Specification of the specimens

Name of Parameters	Symbol	Numerical Values	Unit
Outer diameter for large annular rubber block	OD	37.5459	mm
Inner diameter for large annular rubber block	ID	27.582	mm
Outer diameter for Small annular rubber block	OD	16.78	mm
Outer diameter for Small annular rubber block	ID	3.2134	mm
Permeability	k	2.63 E-10	m^2
Porosity	-	35.7	%
Absolute Viscosity	η	0.116	Pa.s
Nominal Thickness for both specimen	L	2	mm
Initial film thickness	h_0	0.14	mm
Amplitude of vibration	a_s	10	micron

3.3.2.1 Effect of Surface Roughness

Center Line Average (CLA)

In Figure 3.29 hydrodynamic force vs. time curve is plotted under various center line average (CLA) of surface height of rubber block for the frequency 20 Hz. The figure shows that hydrodynamic force developed in the fluid film varies sinusoidally with time due to oscillating motion of the rigid surface over rubber surface. Deformed shape of sinusoidal oscillation curve is not found as in previous case because amplitude of oscillation of rigid plate is very small relative to film thickness. Therefore, amplitude of oscillation has no effect on squeeze time in this case. It is observed that with increasing CLA of surface height the hydrodynamic force increases. This phenomenon is favorable for thrust bearing as high hydrodynamic force contributes to good load carrying capacity.

Similarly Figure 3.30 shows the variation of leakage flow rate with time is under various center line average (CLA) of surface height of rubber block for the frequency 20 Hz. It is seen from the figure that leakage flow rate also varies sinusoidally with time due to oscillating motion of the rigid surface over rubber block. In case of annular rubber block, positive leakage flow indicates that fluid flows outward from the clearance between the mating surfaces. It is also observed that with increasing CLA of the surface height of the rubber block, leakage flow rate decreases slightly which indicates that CLA of surface height of rubber block is not an important parameter in case of seal design.

Standard Deviation (μ)

Variation of the hydrodynamic force with time under various standard deviation of surface height is illustrated in Figure 3.31 for small annular rubber block. Similar to the previous observation, it is seen that with increasing standard deviation hydrodynamic force increases significantly.

36

Leakage flow rate decreases slightly with increasing standard deviation of the surface height of rubber block as shown in Figure 3.32. The reason is that for higher standard deviation of surface height of rubber block fluid gets more restrictions to squeeze out in the finite time which decreases leakage flow rate and huge hydrodynamic force is developed in the fluid film. High hydrodynamic force contributes to good load carrying capacity which is advantageous for thrust bearing.

3.3.2.2 Effect of Permeability

In the Figure 3.33 variation of maximum hydrodynamic force with permeability of rubber block for the frequency 10 Hz is shown. It is observed that with increasing permeability of small annular rubber block hydrodynamic force varies negligibly. Hydrodynamic film force decreases only 1.42% with increasing permeability 10 times. So, effect of permeability of rubber material on load carrying capacity is not significant in case of small annular rubber block used in bearing applications.

3.4 Concluding Remarks

From the observations it can be inferred that surface roughness of rubber block is advantageous in case of bearing, wet clutch and snow tire design as rough surface of rubber block contributes to high load carrying capacity. In case of non-contacting seal design, surface roughness of rubber block can be ignored as it has little effect on leakage flow. Similarly permeability of porous rubber block has significant effect on hydrodynamic force. With the increasing permeability of rubber material, hydrodynamic force film force decreases. This phenomenon contributes to low load carrying capacity. In the previous model by Kaneko *et al.* (2004), analysis of oscillating squeeze film between a rigid surface and porous rubber block is made without considering the effect of permeability and surface roughness of porous rubber block. Therefore, in case of seal design, previous model by Kaneko *et al.* can be applicable for the study of squeeze film characteristics. But in case of bearing design, the effect of surface roughness and permeability of rubber block must be considered.

The effect of surface roughness and permeability of rubber block is considered in the proposed model. So, the proposed model is more accurate than previous Kaneko *et al.*'s model for the analysis of oscillating squeeze film between a rubber surface and a rigid surface in case of both seal and bearing design.
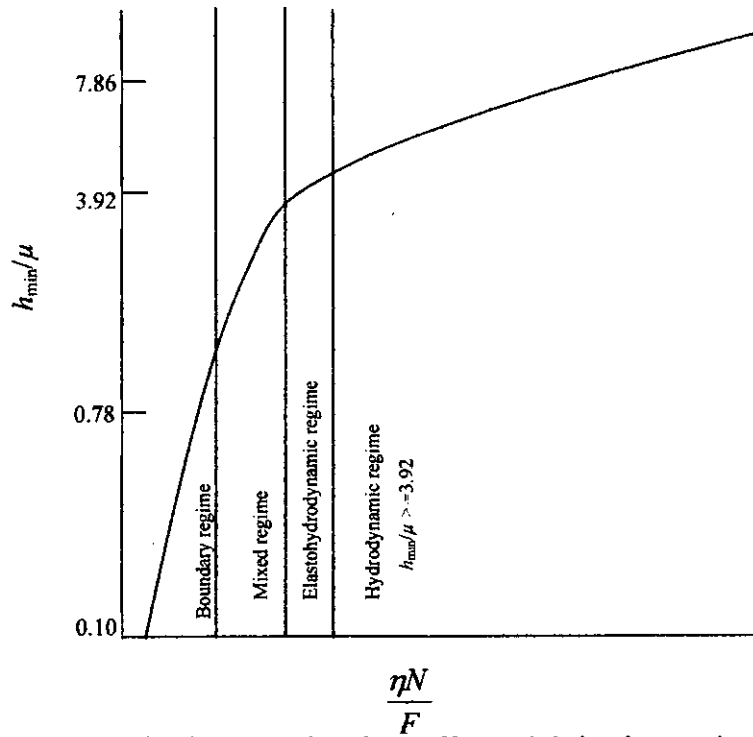
Figure 3.1 Stribeck curve showing different lubrication regimes where N is the rotational speed
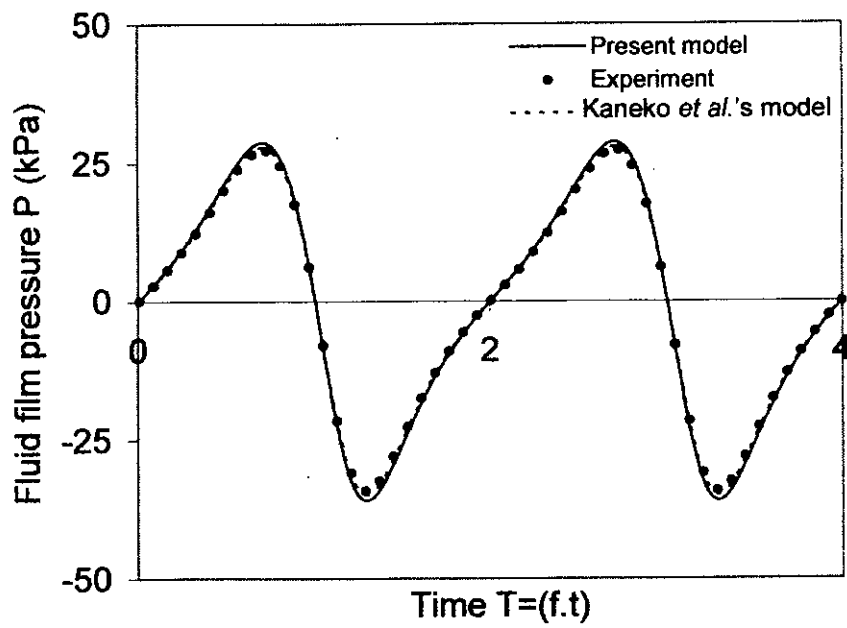
Figure 3.2 Variation of fluid film pressure with time for 20 Hz at the center of the rubber block
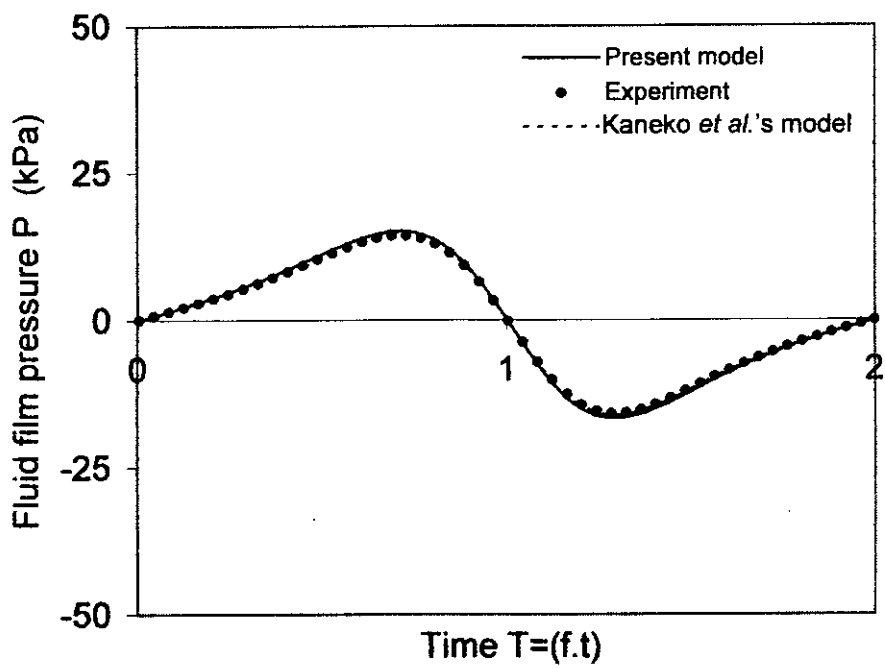
Figure 3.3 Variation of fluid film pressure with time for 10 Hz at the center of the rubber block
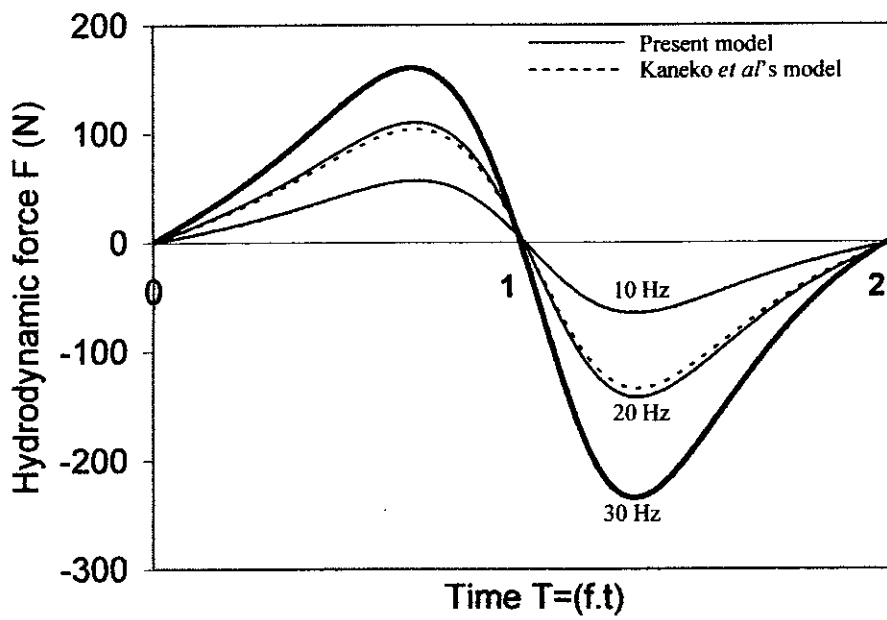
Figure 3.4 Variation of hydrodynamic force with time under various frequencies of oscillation of rigid plate
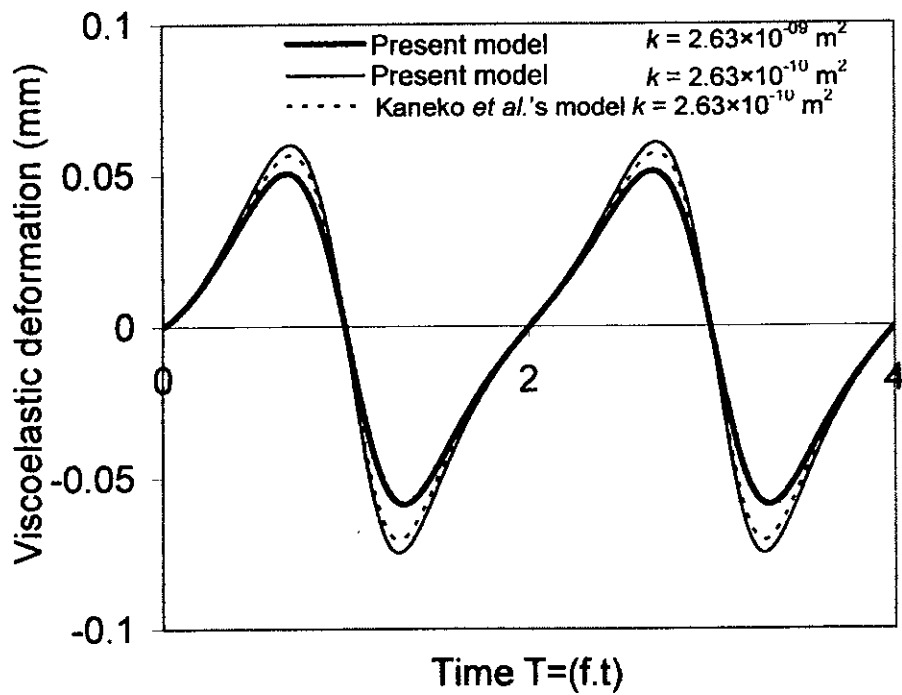
Figure 3.5 Variation of viscoelastic deformation with time for different permeability of porous rubber for 20 Hz at the center of the rubber block
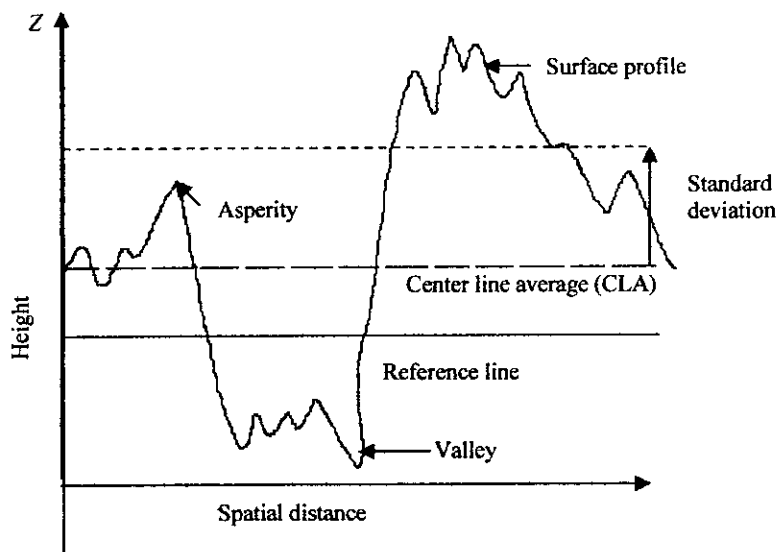
Figure 3.6 Schematic diagram of surface profile
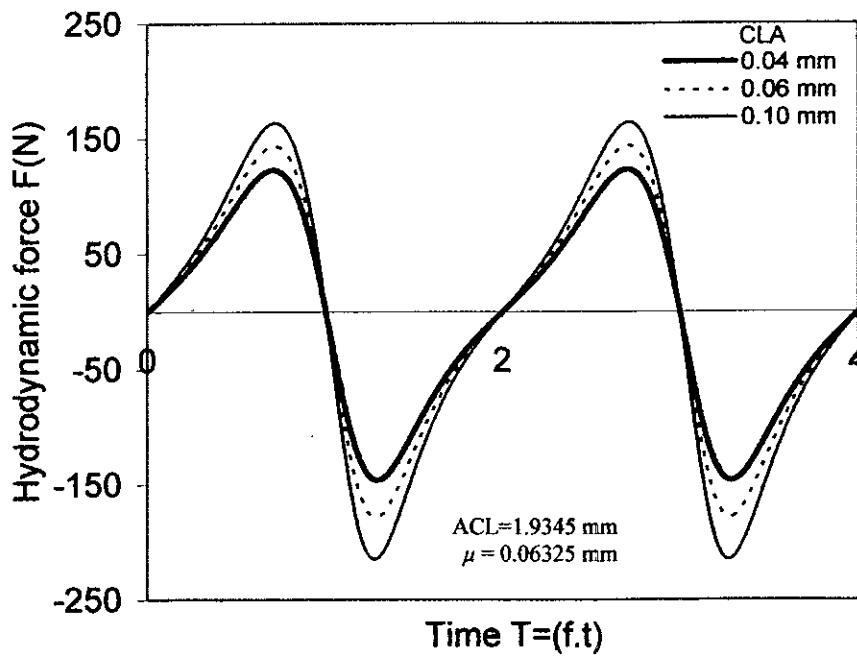
Figure 3.7 Variation of hydrodynamic force with time for various CLA of surface height of rubber block for 20 Hz
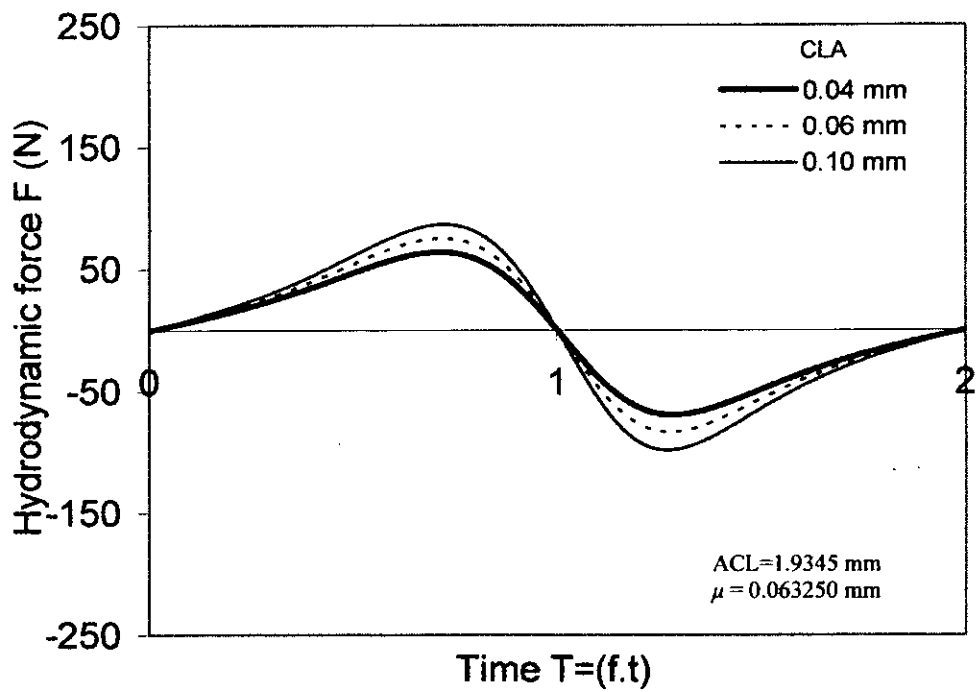
Figure 3.8 Variation of hydrodynamic force with time for various CLA of surface height of rubber block for 10 Hz
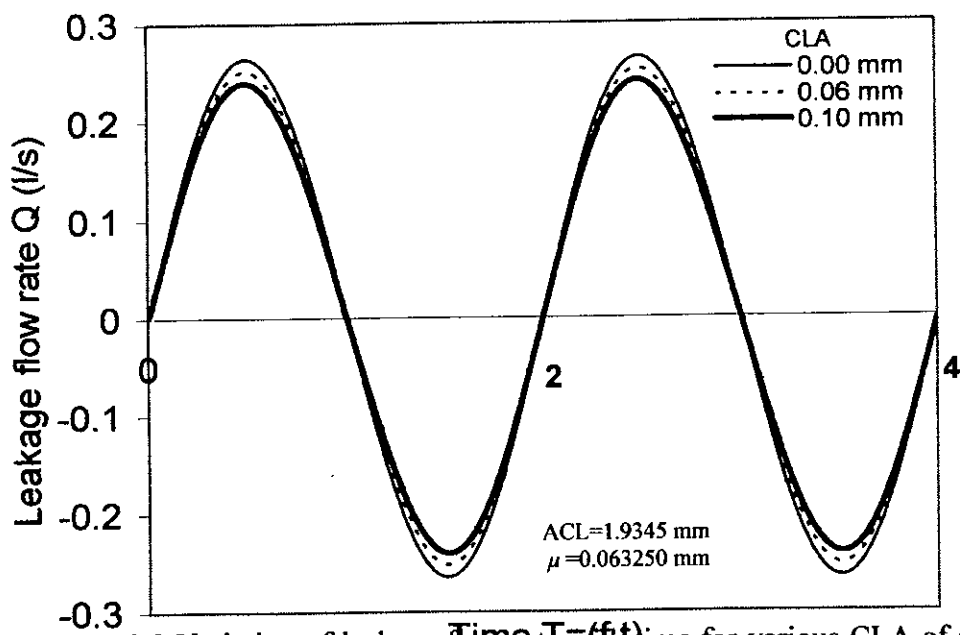
Figure 3.9 Variation of leakage flow rate with time for various CLA of surface height of rubber block for 20 Hz
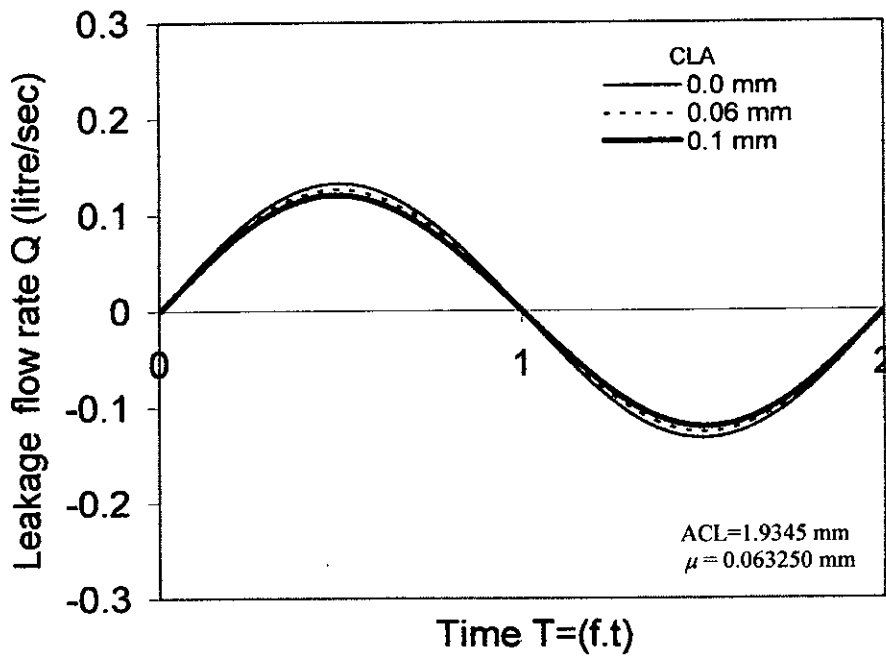
Figure 3.10 Variation of leakage flow rate with time for various CLA of surface height of rubber block for 10 Hz
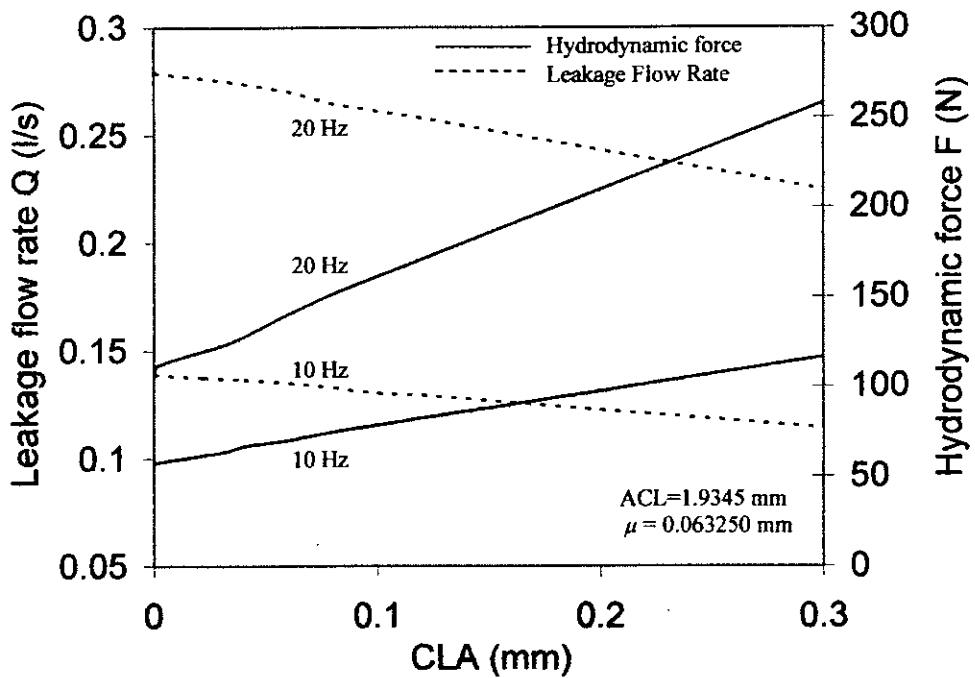
Figure 3.11 Variation of maximum leakage flow rate and hydrodynamic force with center line average (CLA) of surface height of rubber block for different frequencies
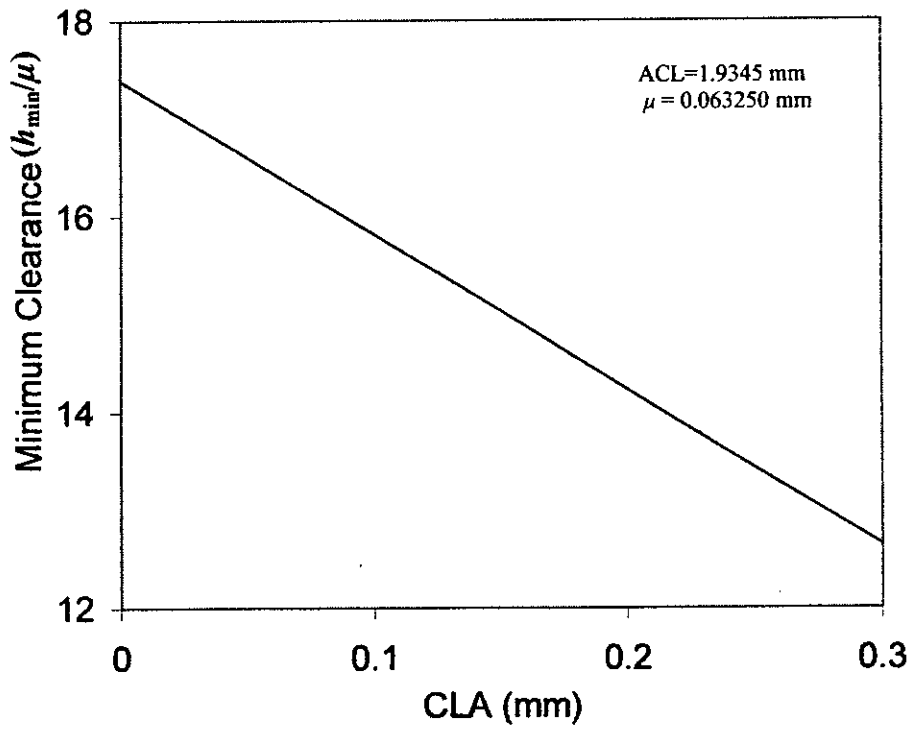
Figure 3.12 Variation of minimum clearance (h_{min}/μ) with different CLA of surface height of rubber block
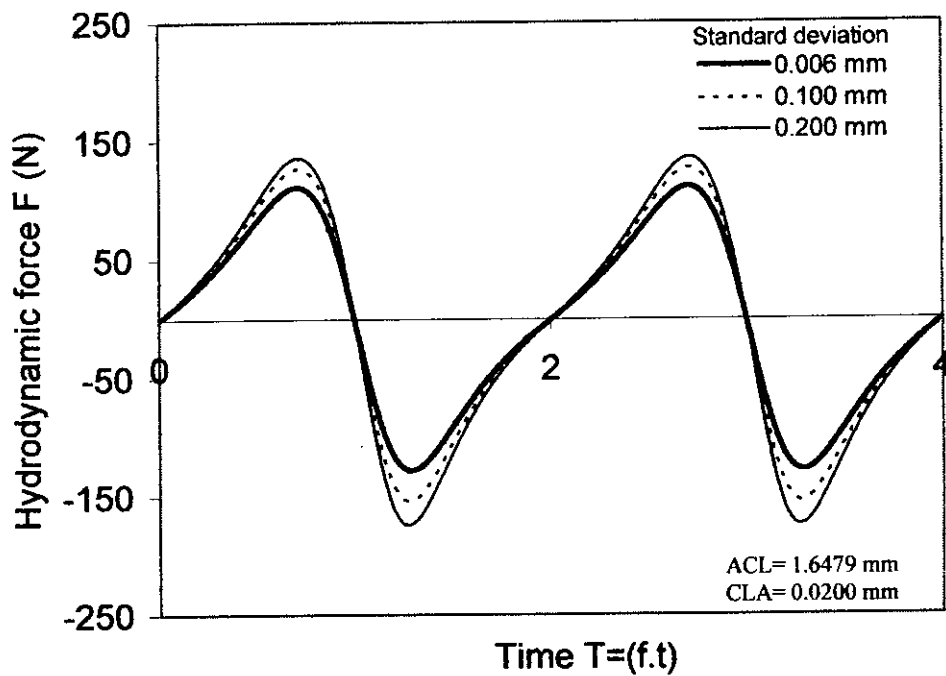
Figure 3.13 Variation of hydrodynamic force with time under various standard deviation of surface height of rubber block for 20 Hz
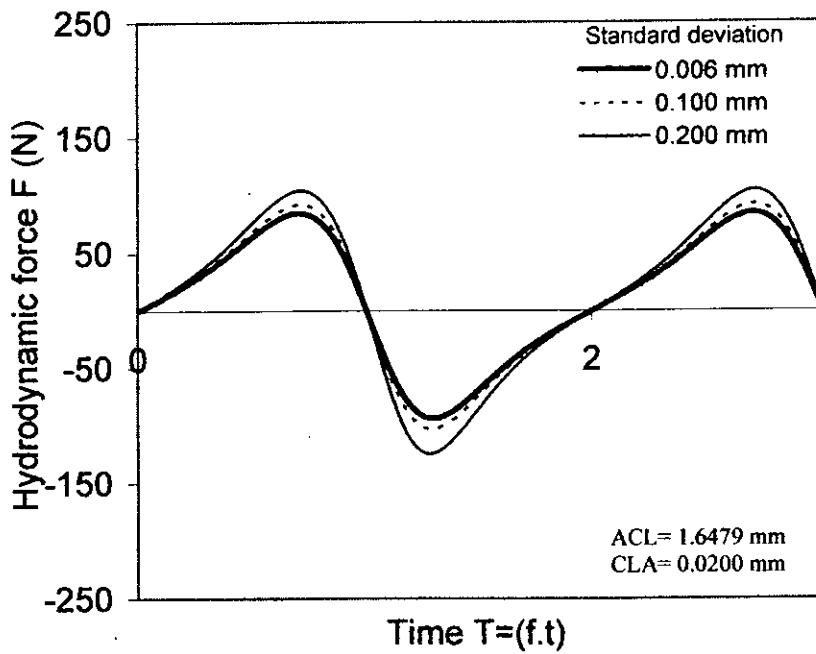
Figure 3.14 Variation of hydrodynamic force with time under various standard deviation of surface height of rubber block for 15 Hz
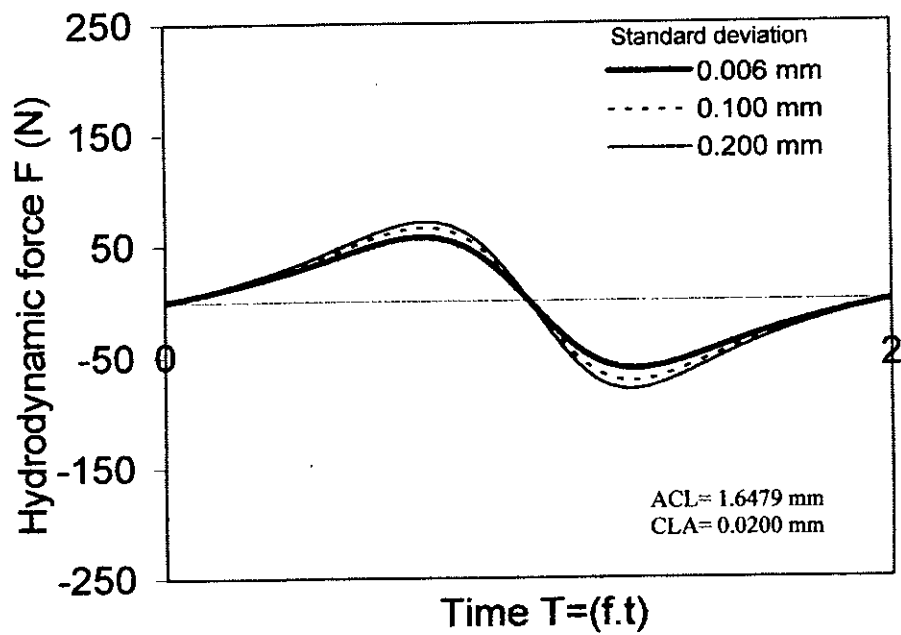
Figure 3.15 Variation of hydrodynamic force with time under various standard deviation of surface height of rubber block for 10 Hz
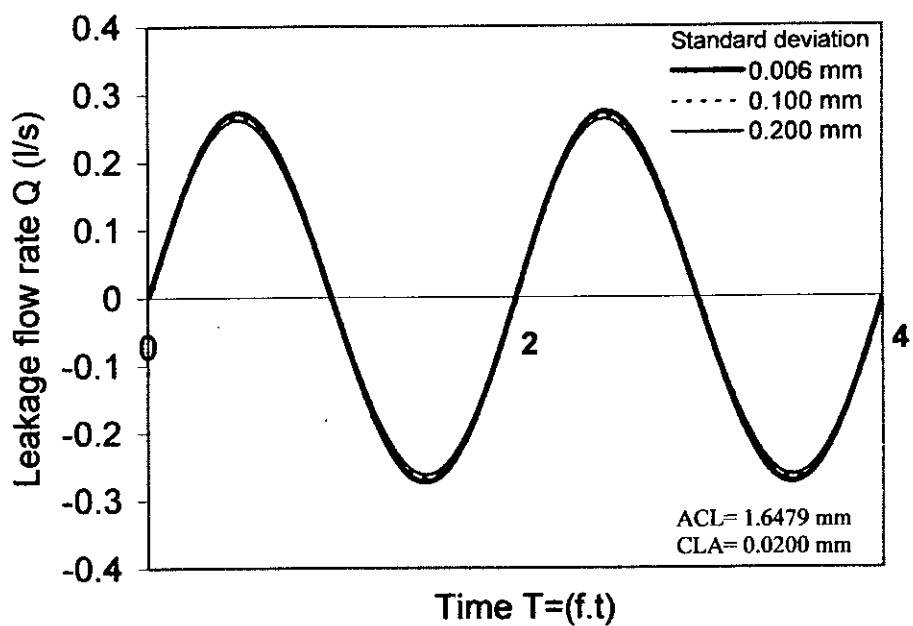
Figure 3.16 Variation of leakage flow rate with time under various standard deviation of surface height of rubber block for 20 Hz
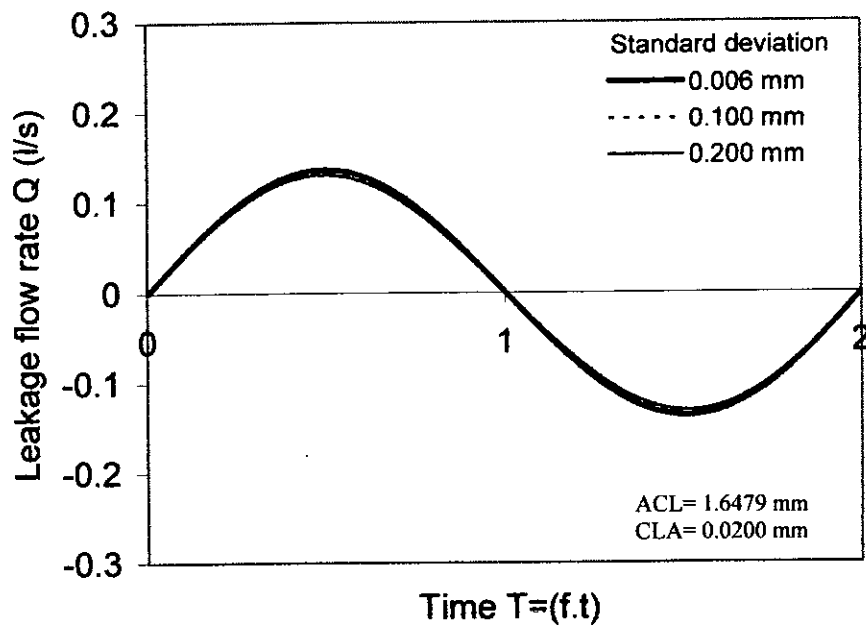
Figure 3.17 Variation of leakage flow rate with time under various standard deviation of surface height of rubber block for 10 Hz
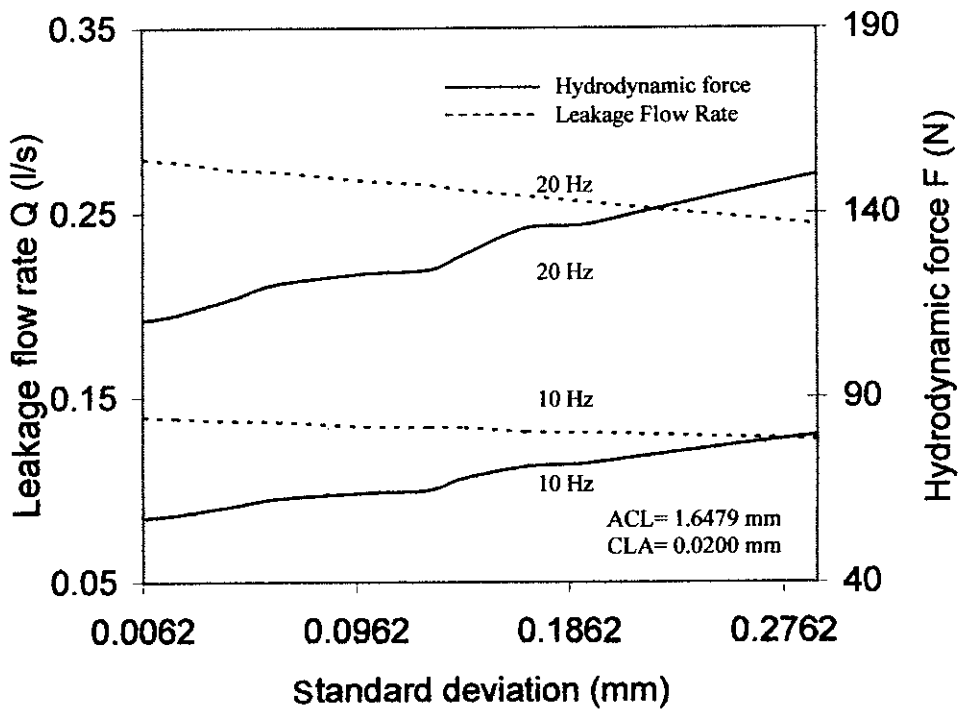
Figure 3.18 Variation of maximum leakage flow rate and hydrodynamic force with standard deviation of surface height of rubber block for different frequencies
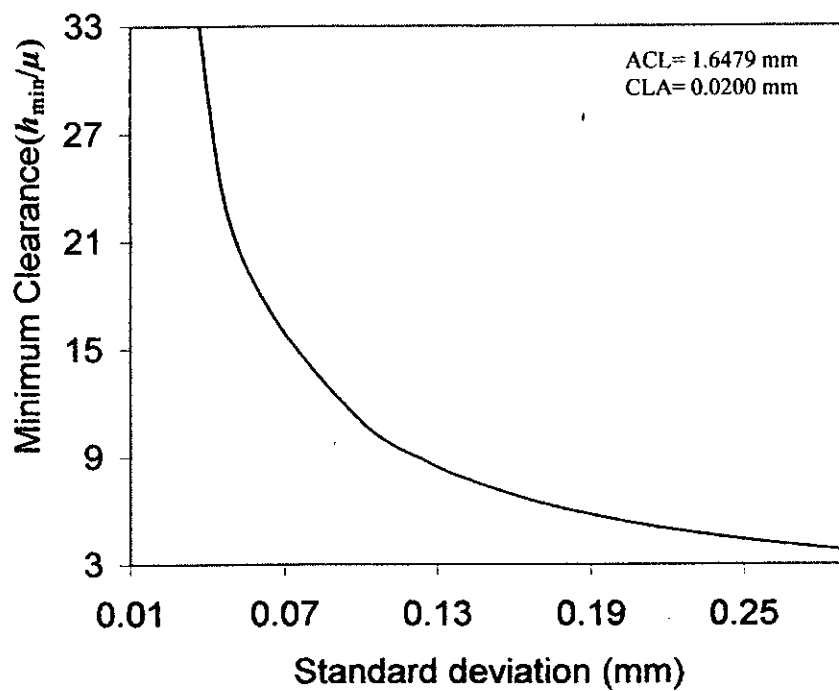
Figure 3.19 Variation of minimum clearance (h_{min}/μ) with standard deviation of surface height of rubber block

Standard deviation = 4.37 nm & β^*=1.01 μm

Standard deviation = 4.18 nm & β^*=6.04 μm
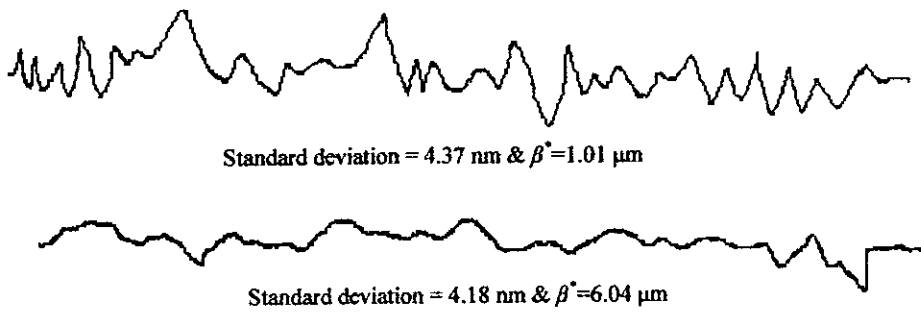
Figure 3.20 Two dimensional rough surfaces of different spatial distribution
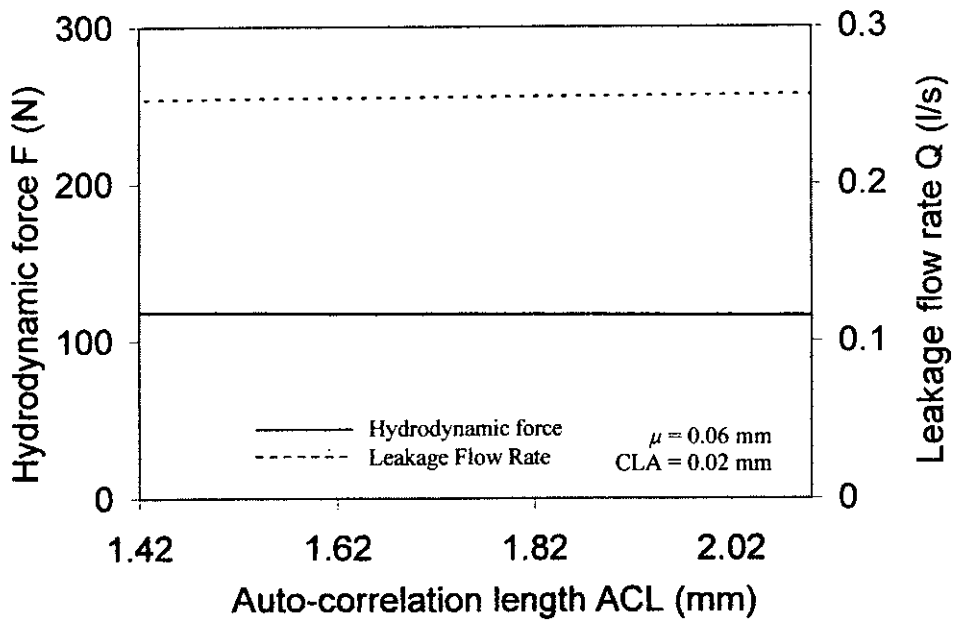
Figure 3.21 Variation of maximum hydrodynamic force and leakage flow rate with auto correlation length (ACL) of rubber surface
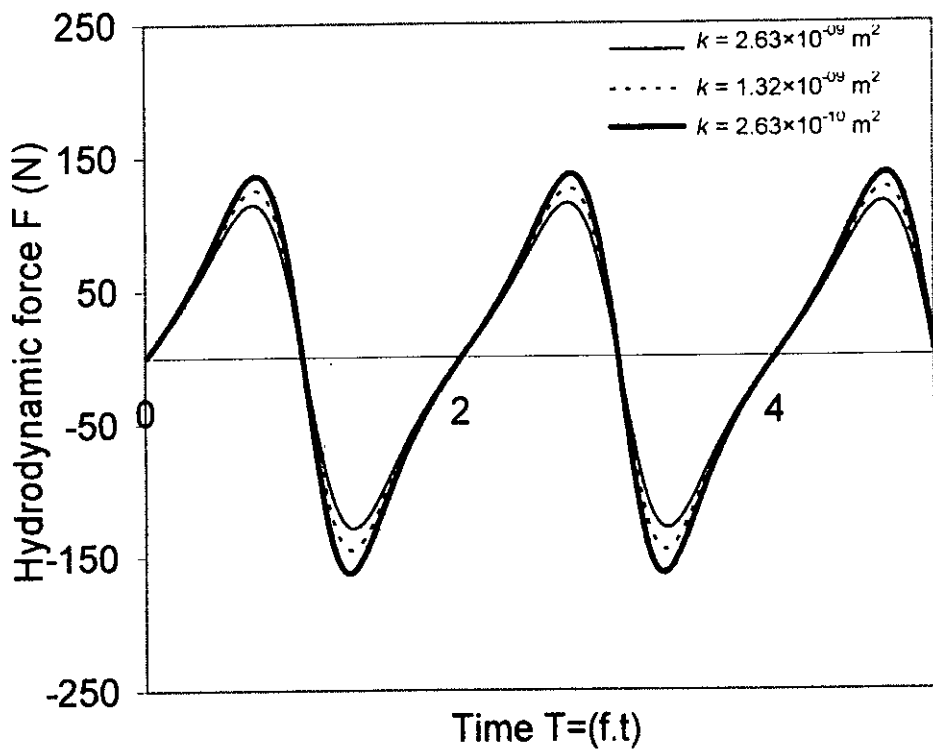
Figure 3.22 Variation of hydrodynamic force with time under various permeability of porous rubber for 25 Hz
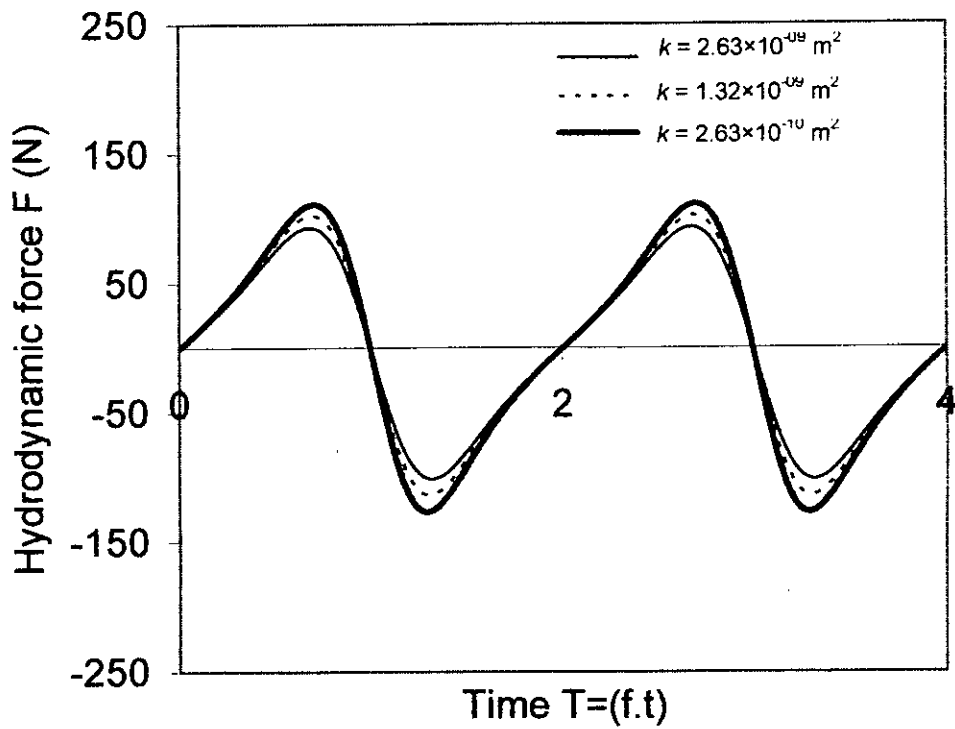
Figure 3.23 Variation of hydrodynamic force with time under various permeability of porous rubber for 20 Hz
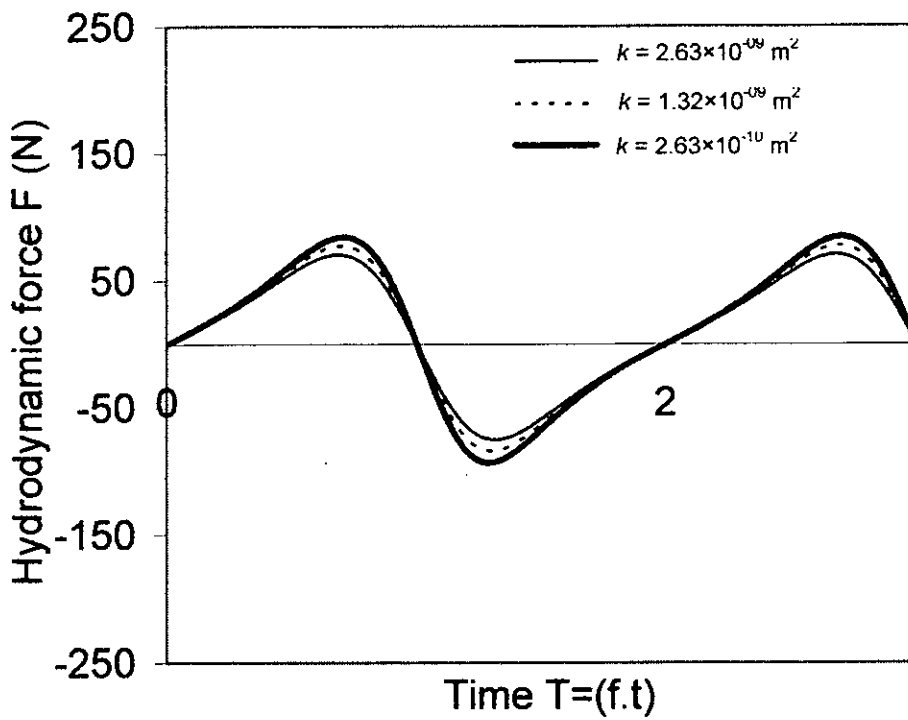
Figure 3.24 Variation of hydrodynamic force with time under various permeability of porous rubber for 15 Hz
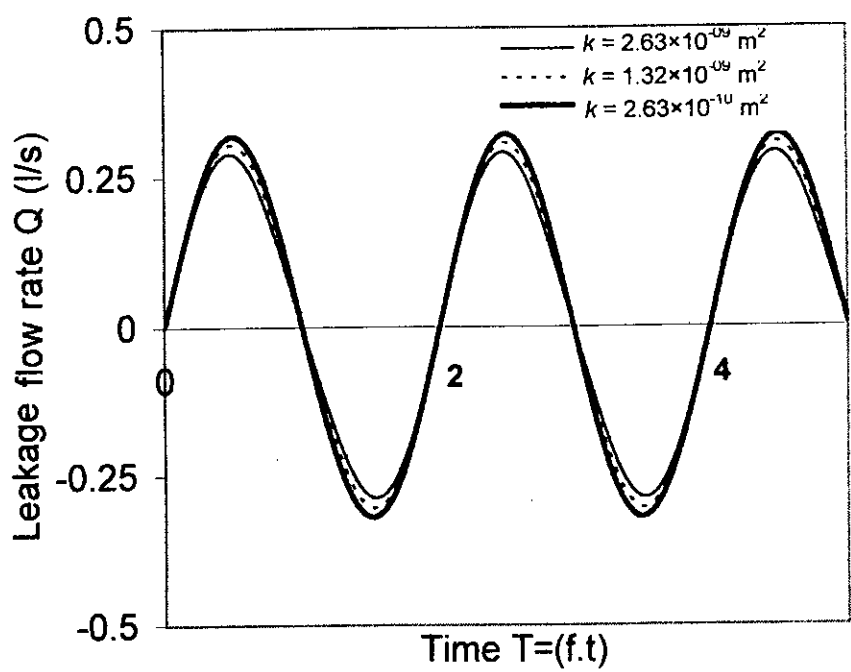
Figure 3.25 Variation of leakage flow rate with time under various permeability of porous rubber for 25 Hz
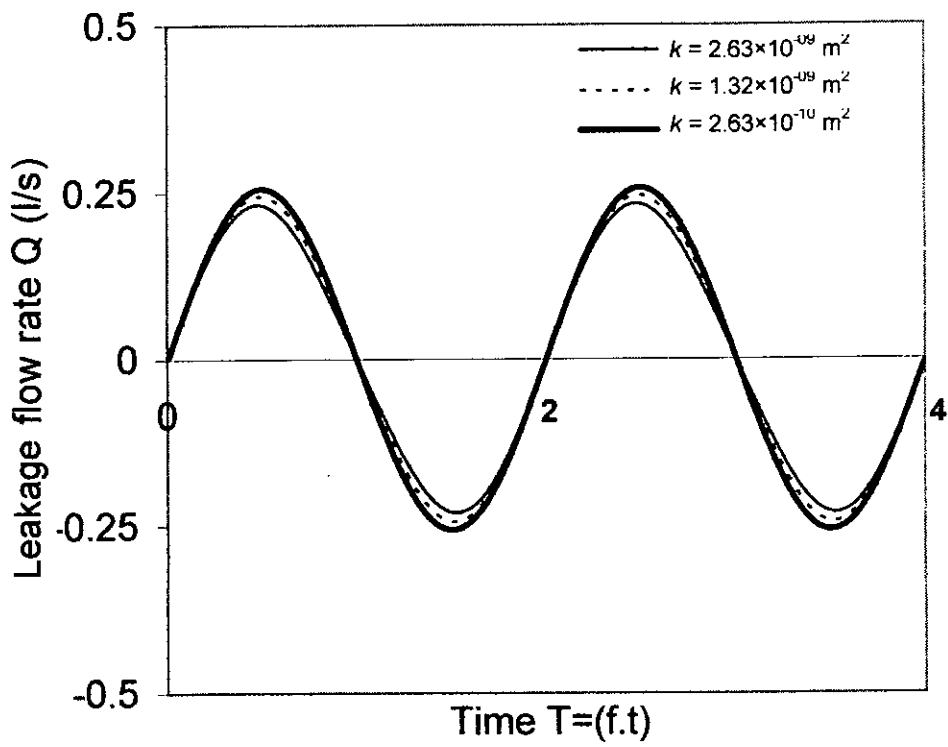
Figure 3.26 Variation of leakage flow rate with time under various permeability of porous rubber for 20 Hz
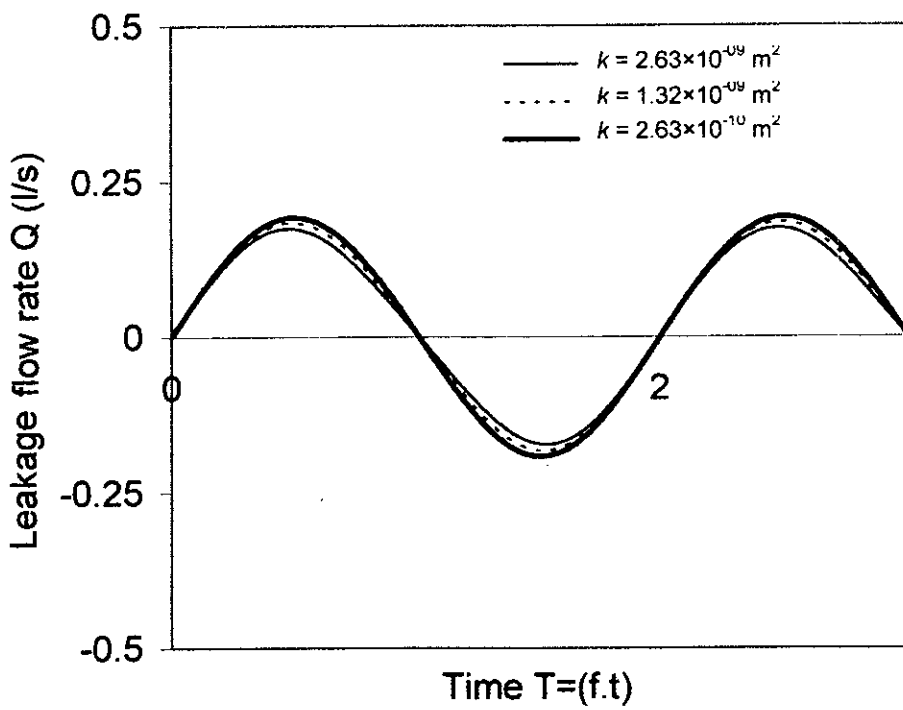
Figure 3.27 Variation of leakage flow rate with time under various permeability of porous rubber for 15 Hz
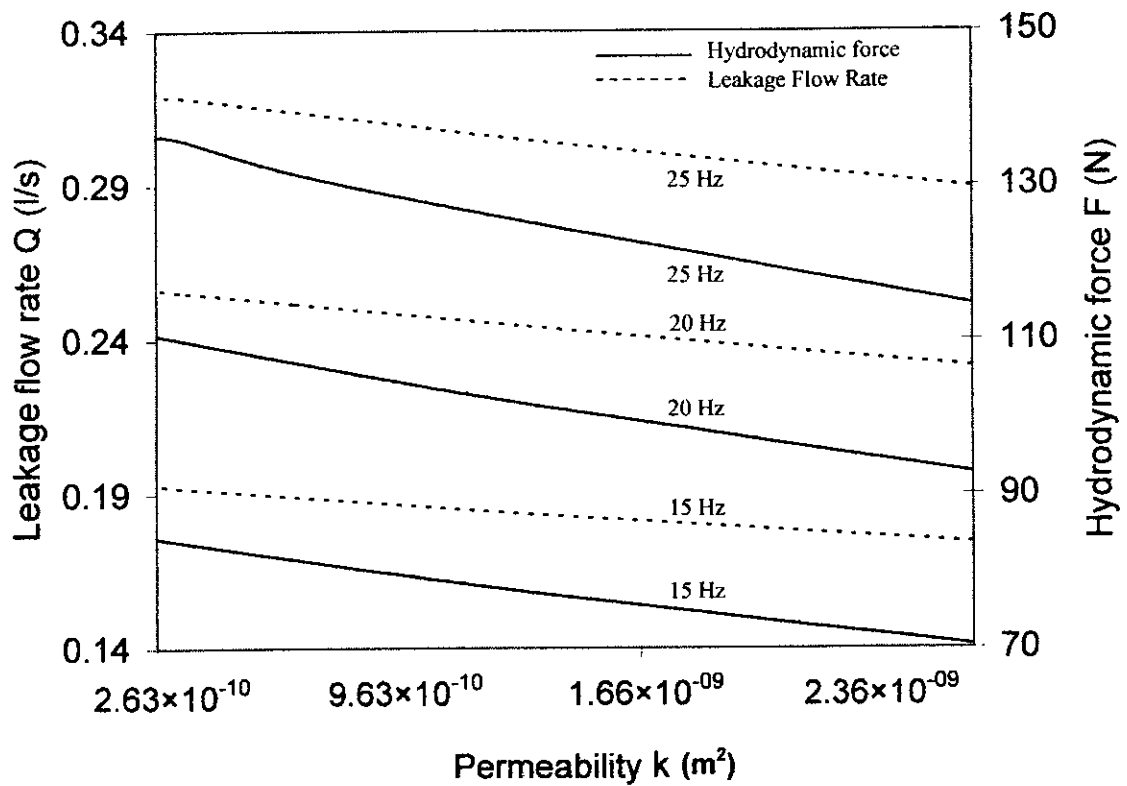
Figure 3.28 Variation of maximum leakage flow rate and hydrodynamic force with permeability of porous rubber block for different the frequencies
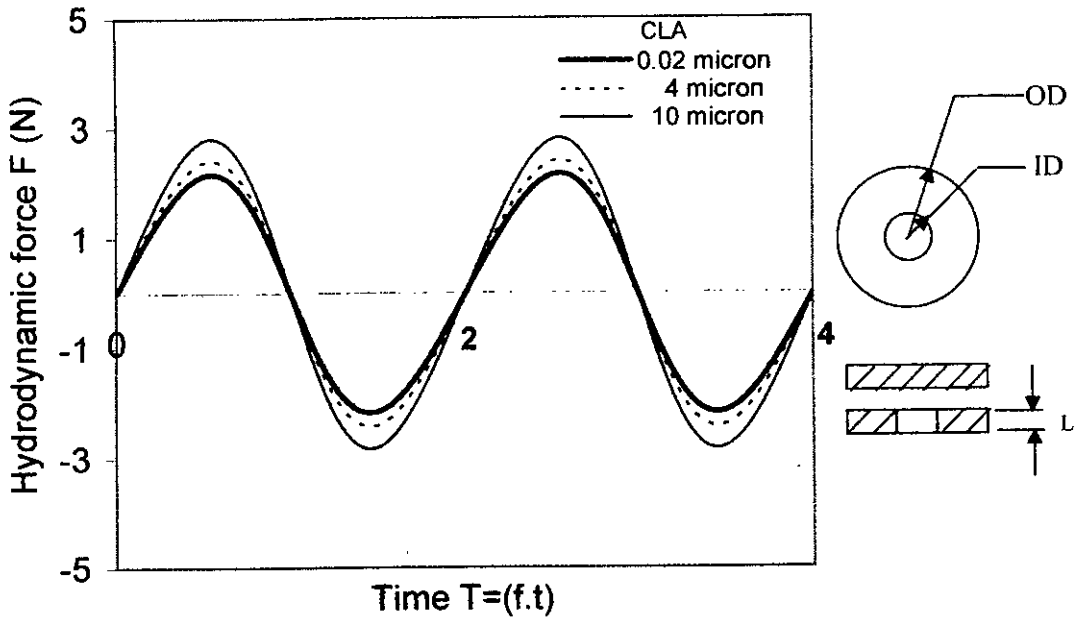
Figure 3.29 Variation of hydrodynamic force with time under different CLA of surface height of rubber block for 20 Hz for annular rubber block (L = 2 mm, OD = 37.5459 mm, ID = 27.582 mm, ACL = 0.39338 mm and μ = 0.006325 mm)
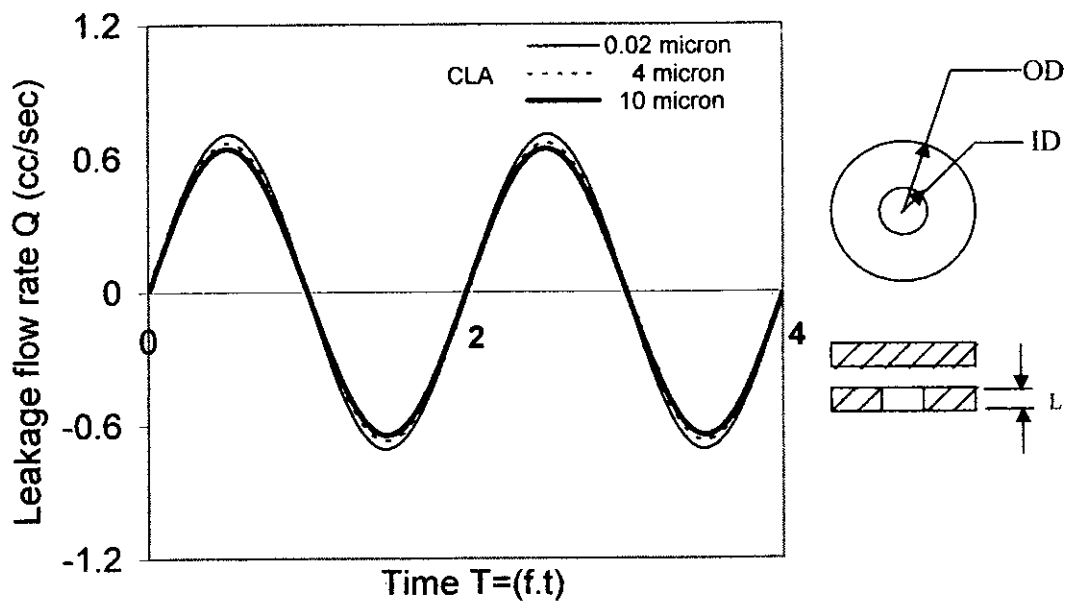
Figure 3.30 Variation of leakage flow rate with time under different CLA of surface height of rubber block for 20 Hz for annular rubber block (L = 2 mm, OD = 37.5459 mm, ID = 27.582 mm, ACL = 0.39338 mm and μ = 0.006325 mm)
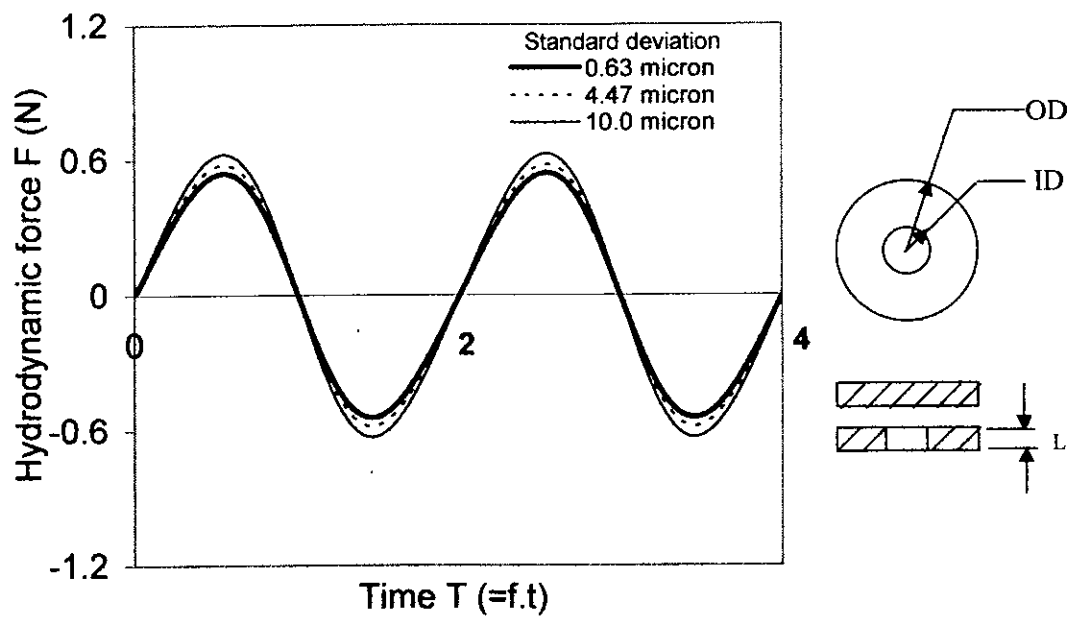
Figure 3.31 Variation of hydrodynamic force with time under various standard deviation of surface height of rubber block for 20 Hz for annular rubber block (L = 2 mm, OD = 16.78 mm, ID = 3.2134 mm, ACL = 0.45627 mm and CLA = 0.02 mm)
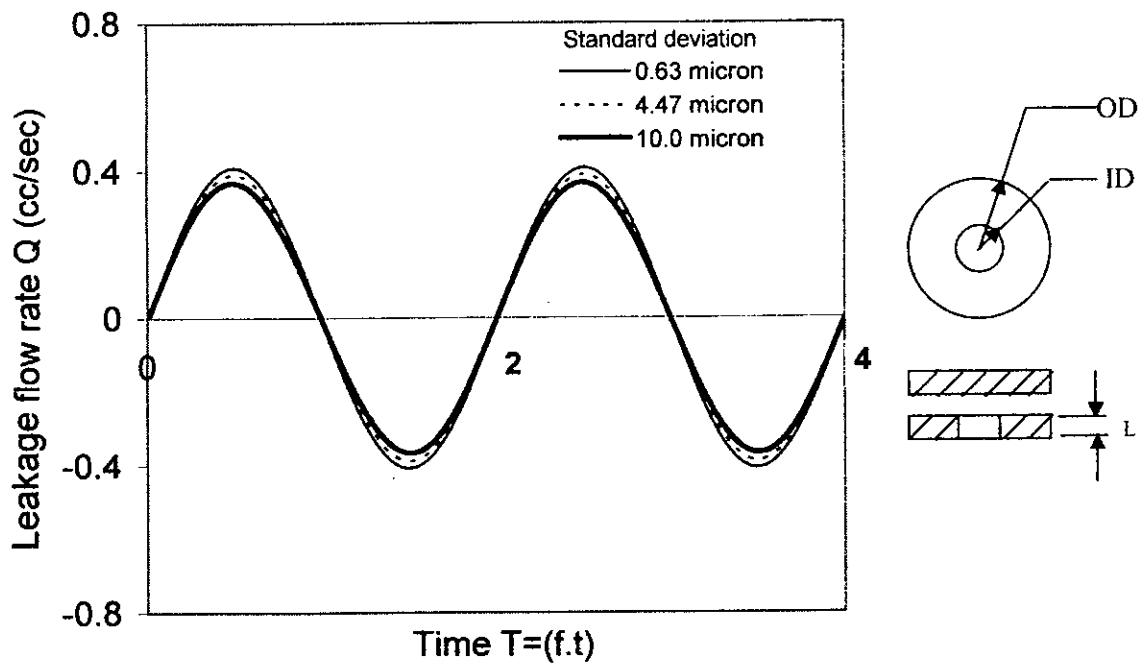
Figure 3.32 Variation of leakage flow rate with time under various standard deviation of surface height of rubber block for 20 Hz for annular rubber block (L = 2 mm, OD = 16.78 mm, ID = 3.2134 mm, ACL = 0.45627 mm and CLA = 0.02 mm)
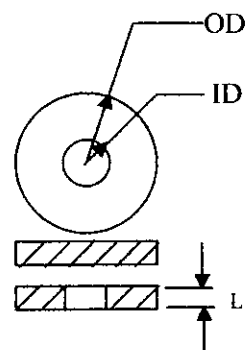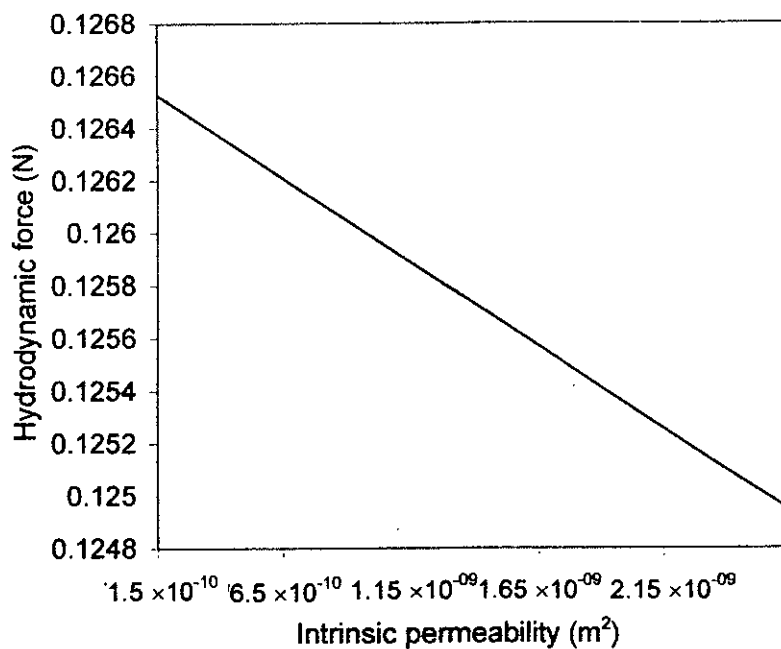
Figure 3.33 Variation of maximum hydrodynamic force vs. permeability of porous rubber block for 10 Hz (L=2 mm, OD=16.78 mm & ID=3.2134 mm, ACL=0.39338 mm, standard deviation =0.006325 mm & CLA=0.0 mm)

Chapter 4

Conclusions

4.1 Introduction

As mentioned in Chapter 1, the main objective of the present study was to analyze the squeeze behavior between an oscillating rigid plate and a porous rubber block under various frequencies of oscillation, surface roughness of rubber surface and different values of permeability of rubber block. Effects of surface roughness on hydrodynamic force, minimum clearance and leakage flow rate are shown varying two dimensional surface texture characteristics parameters: center line average (CLA), standard deviation and auto-correlation length. Effects of permeability of rubber block on hydrodynamic film force and leakage flow rate are also shown in the previous chapter. Both solid and annular rubber blocks are considered for the analysis. It is inferred that surface roughness and permeability of rubber block have a significant effect on load carrying capacity but have a negligible effect on leakage flow rate. Kaneko *et al.*'s (2004) model can be applicable only in case of seal design as analysis of oscillating squeeze film between a rigid surface and porous rubber block is made without considering the effect of permeability and surface roughness of rubber block. But accurate result can not be obtained from Kaneko *et al.*'s model in case of bearing design. Both effect of surface roughness and permeability of rubber block are considered in the proposed model. Therefore, the proposed model is more effective than the previous Kaneko *et al.*'s model for the analysis of oscillating squeeze film between a rubber surface and a rigid surface in case of both seal and bearing design.

4.2 General Conclusion

The following facts have emerged from the analysis of computational results.

1. Frequency of the oscillating motion significantly affects leakage flow rate and hydrodynamic force. With increasing frequency of oscillation hydrodynamic film force as well as leakage flow rate increases.

2. There are significant effects of surface roughness of rubber on leakage flow rate and hydrodynamic force. It is investigated that with increasing center line average (CLA) of surface height huge hydrodynamic film force is developed in the fluid film which contributes to good load carrying capacity. It has been seen from theoretical analysis that leakage flow rate reduces to 19% for increasing center line average from 0 mm to 0.3 mm where as hydrodynamic film force increases 2 times for frequency 20 Hz. This infers that CLA of surface height of rubber block has significant effect on load carrying capacity but less effect on leakage flow rate.

3. There are also significant effects of standard deviation of surface height on hydrodynamic force and load carrying capacity and less effect on leakage flow rate. From the observation as described in the previous chapter that for increasing standard deviation of surface height from 0.0062 mm to 0.29 mm hydrodynamic film force increases 36% where as leakage flow rate reduces to 18 % for frequency 20 Hz.

4. It has been seen that permeability of porous rubber block can affect mostly hydrodynamic film force and load carrying capacity. With increasing permeability hydrodynamic force decreases due to the seepage flow across the porous material. As mentioned in the previous chapter it has been seen that for frequency 25 Hz leakage flow rate decreases only 6.6% where hydrodynamic film force decreases to 25%. It indicates that permeability mostly affects the hydrodynamic force and has less effect on leakage flow rate. Therefore,

permeability of rubber block must be considered in case of bearing and wet clutch design.

5. With increasing center line average (CLA) and standard deviation of surface height minimum clearance decreases which reduces leakage flow rate. This phenomenon is mostly attractive in case of non-contacting seal design. But optimization must be required as if seal clearance (h_{min}/μ) goes below 3.92 there is possibility of more frequent contacts between the mating surfaces and degrades the quality of seal materials like rubber.

6. Auto-correlation length of surface roughness of rubber has no significant influence on leakage flow rate and hydrodynamic force. So, in case of bearing, snow tire, wet clutch and non-contacting seal design height distribution of surface texture play a significant role than spatial distribution of surface texture.

In conclusion, it is clear that for bearing, snow tire and wet clutch used in many engineering and industrial purposes, surface roughness of deformable porous material like rubber has much advantageous because it increases load carrying capacity. Also due to surface roughness huge hydrodynamic force is developed in fluid film between the mating surfaces which is also advantageous for non-contacting seal to maintain proper oil film between the mating surfaces. Despite of this advantage, surface roughness can be ignored for the simplification of numerical modeling in case of seal design. Similarly, permeability of rubber block has significant effect on load carrying capacity. With increasing permeability of porous rubber block, load carrying capacity decreases. Therefore, the value of permeability of rubber material should be optimized in case of bearing and wet clutch design.

4.3 Recommendation for Future Works

On the basis of the experience gained during this study, the following suggestions for future works can be made:

1. In the present work input properties for oil film are assumed independent of temperature. But seals used in industrial purposes can be operated at much higher temperature than the assumed value in the present model. Properties of lubricating oil will be varying with temperature. Therefore, temperature can be considered in the present modeling which will be more realistic for analysis.

2. Viscoelastic deformation of rubber material is considered in the present modeling. Thermal distortion of rubber surface may be included in the present model for the seals operated at higher temperature.

3. During suction occurred between the mating surfaces pressure may go down below the oil vapor pressure for higher frequency of oscillating motion which may cause cavitation phenomenon. Bubbles form between the mating surfaces and collapse during squeezing. Therefore, multi-phase phenomena may be considered in future work.

4. Effect of amplitude of oscillation of rigid plate on hydrodynamic force and leakage flow rate can be analyzed in future work.

References

Stribeck, R.(1902), Characteristics of plain and roller bearings, *Zeit. Ver. Deut. Ing.* 46, 1341-1348, 1432-1438, 1463-1470.

Kozeny, B. (1966), *Heat and Mass Transfer in Capillary-porous Bodies*, Pergamon Press, London.

Sneak, H. J.(1968), The effect of geometry and inertia on face seal performance-turbulent flow, *ASME J. Lub. Tech.*, 342-350.

Cheng, H. S., Chow, C. Y. and Wilcock, D. F. (1968), Behavior of hydrostatic and hydrodynamic noncontacting face seals, *ASME J. Lub. Tech.*, 510-518.

Sneak, H. J. (1968), The effect of geometry and inertia on face seal performance-laminar flow, *ASME J. Lub. Tech.*, 333-340.

Wu, H. (1970), Squeeze-film behavior for porous annular disks, *ASME J. Lub. Tech.*, 92, 593-596.

Murti, P. R. K. (1974), Squeeze-film behavior in porous circular disks, *J. Lub. Tech.*, 74, 206-209.

Ting, L. L. (1975), Engagement behavior of lubricated porous annular disks, *Wear*, 34, 159–182.

Rodhe, S. M., Whicker, D. and Booker, J. F. (1979), Elastohydrodynamic squeeze films: effects of viscoelasticity and fluctuating loading, *ASME J. Lub. Tech.*, 101, 74-80.

Hori, Y. and Kato, T. (1979), A study of viscoelastic squeeze films, *JSLE Trans.*, 24(3), 174-181.

Lai, T. W. (1980), Development of non-contacting, non-leaking spiral groove liquid face seals, *Lub. Engg.*, 50 (8), 625-640.

Hori, Y., Kato, T. and Narumiya, H. (1981), Rubber surface squeeze film, *ASME J. Lub. Tech.*, 103, 398-405.

Snegovsky, F. P., Buljuk, N.G. (1983), Study of lubrication of sliding bearings with microcavities on journals, *Friction and Wear*, 4(2), 321-328.

Wada, S., and Nishida, S.(1985), Elastohydrodynamic lubrication of porous squeeze bearings with non-newtonian fluids, *Trans. Jpn. Soc. Mech. Eng.*, Ser. C, 51(469), 2183-2190.

Yoo, H. S. (1987), Some effects of viscoelastic matrix on the squeeze films, *ASLE Trans.*, 30, 403-408.

Ikeuchi, K., Oka, M. and Mori, H. (1989), A simulation of the squeeze film effect in a hip joint, *Trans. Jpn. Soc. Mech. Eng.*, Ser. C, 55(510), 508-515.

Ikeuchi, K., Oka, M. and Gi, K. (1989), An experimental study of deformation and squeeze film effect in a synovial joint, *Trans. Jpn. Soc. Mech. Eng.*, Ser. C, 55(516), 2123-2130.

Horikawa, J., Kyogoku, T. and Nakahara, T. (1990), Lubrication characteristics with porous elastic materials: numerical analysis, *Proc. JAST.*, 377-380.

Ahmad, M. M. H. M., Gethin, D. T., Claypole, T. C. and Roylance, B. J. (1998), Numerical and experimental investigation into porous squeeze films, *Tribology International*, 31, 189-199.

Lin, J. R., Hsu, C. H. and Chuan, L. (2002), Surface roughness effects on the oscillating squeeze-film behavior of long partial journal bearings, *Computers & Structures*, 80, 297-303.

Kaneko, S., Tanaka, T., Abe, S. and Ishikawa, T. (2004), A study on squeeze films between porous rubber surface and rigid surface: analysis based on the viscoelastic continuum model, *J. Tribology*, 126, 719-727.

Burjurke, N. M., Naduvinamani, N. B., Fathima, S. T. and Benchalli, S. S. (2006), Effect of surface roughness on couple stress film lubrication of long porous partial journal bearings, *Industrial Lubrication and Tribology*, 58, 176-186.

Appendix A

Basic Concepts

A.1 Surface Topography

Increasing production speeds and new cutting methods, such as plasma cutting, spark erosion and laser cutting, change the characteristics of machined surfaces. Requirements with regard to surface accuracy and surface refinement have also greatly increased. The importance of a fine-scale surface description is well mentioned in tribology. The breakdown of lubrication layers of oil in engine cylinders or in bearings can be improper micro level surface shape. Although bearing design theory and lubrication engineering relies heavily on fluid mechanics and kinematics, surfaces texture can be still important in ensuring proper lubrication.

A.2 Geometric Characteristics of Surfaces

The geometry characteristics, or texture, of surface as shown in figure A.1 may be divided into three main categories:

1. *Error of form.* The surface deviates from a well-defined pattern because of errors inherent in the manufacturing process.
2. *Waviness.* Relatively long waves in a surface profile are often associated with unwanted vibrations that always occur in machine tool systems.
3. *Roughness.* Irregularities, excluding waviness and error of form, are inherent in the cutting and polishing process during production.

In the study of lubricated surfaces, roughness is the geometry variation that is generally of interest. Although often no sharp distinction can be drawn between these categories, roughness simply concerns the horizontal spacing (wave length) of surface features. From a practical point of view, in characterizing surface used in tribology both the vertical direction (and amplitude) and the horizontal direction (or wavelength) are important.

| Actual surface profile | Error of form | Waviness | Roughness |
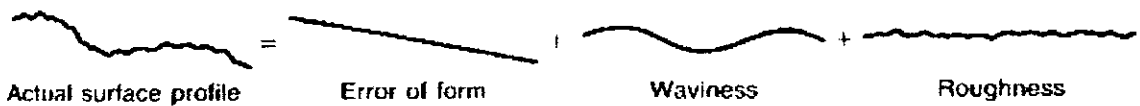
Figure A.1 Geometric characteristics of solid surfaces [From Halling (1976)]

A.3 Typology of Surfaces

The characteristics of the topography of solid surfaces are of interest in the study of a number of interfacial phenomena such as friction, wear, electrical and thermal contact resistance. A very general typology of solid surfaces is shown in Figure A.2. Surfaces that are deterministic may be studied by relatively simple analytical and empirical methods; their detailed characterization is straightforward. However, many engineering surfaces are random and these have been subjected to a great deal of study in the past decade. In the present thesis paper, attention is concentrated on random, isotropic, Gaussian surfaces, although extensions of the theory to non-isotropic surfaces are also indicated here. It is clear that many surfaces are non-Gaussian but it is equally clear that many engineering surfaces are Gaussian. Moreover, a study of Gaussian surfaces should provide a good preparatory background for the study of non-Gaussian surfaces.

79

```
                        Solid surface
                             |
                             v
        ┌────────────────────┴────────────────────┐
        v                                          v
  Inhomogeneous                              Homogeneous
                                                   |
                                  ┌────────────────┴────────────────┐
                                  v                                 v
                            Deterministic                        Random
                                                   ┌───────────────┴───────────────┐
                                                   v                               v
                                                Gaussian                     Non-Gaussian
                                                   |
                                  ┌────────────────┴────────────────┐
                                  v                                 v
                              Isotropic                       Non-isotropic
```
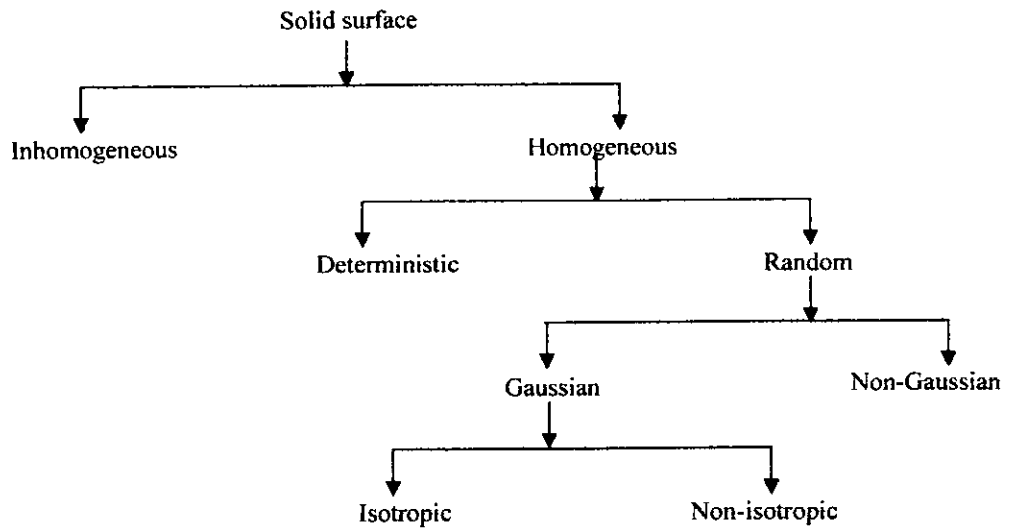
Figure A.2 Typology of surfaces

A.4 Gaussian Rough Surface Parameters

A two dimensional Gaussian isotropic surface can be simply characterized by two functions: Height distribution and spatial distribution.

A.4.1 Height Functions

It is usually characterized by one of the two statistical height descriptors advocated by the American National Standards Institute (ANSI) and International Standardization Organization (ISO). These are:

1. R_a, CLA (Center Line Average) or AA (arithmetic mean): Center line is defined as the line such that the area between the profile and the mean line above the line is equal to the below the mean line. R_a, CLA or AA is the arithmetic mean of the absolute values of vertical deviation from the mean line through the profile. Mathematically,

$$R_a = CLA = \frac{1}{L} \int_0^L |z - m| dx$$

2. Standard Deviation (μ): The standard deviation (μ), is the square root of the arithmetic mean of the square of the vertical deviation from the mean line. It denotes the mean deviation form the center line. In many case deviation of the surface height can be expressed as variance as,

$$\mu^2 = \frac{1}{L} \int_0^L (z - m)^2 dx$$

where μ is the standard deviation.

A.4.2 Spatial Function

Various rough surface having same R_a and μ may show different spatial arrangements of surface heights. Slope and curvature distributions are not, in general, sufficient to represent the surface, as they refer only to one particular spatial size of features. The special functions namely the auto covariance or auto correlation function (ACVF), structure function (SF) or power spectral density function (PSDF), offer a means of representing the properties of all wavelength or spatial sizes of the features. These are known as surface texture descriptors. ACVF or ACF has been the most popular way of representing spatial variation. In the present study, attention is concentrated on ACF to describe the spatial arrangement of surface height.

Autocovariance and autocorrelation Functions: For a function z(x), the ACVF for spatial separation of τ is an average value of the product of two measurements taken on the profile a distance τ apart, z(x) and z(x+ τ). It is obtained by comparing the function z(x) with a replica of itself where the replica is shifted an amount τ as in figure A.3
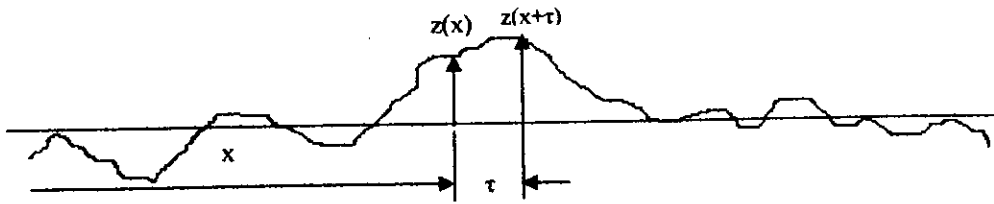
Figure A.3 Construction of auto covariance function

where L is the sampling length of the profile. From its definition, ACVF is always an even function of τ that is,

$$R(\tau) = R(-\tau)$$

The normalized form of the ACVF is called the auto correlation function (ACF) and is given

$$C(\tau) = \lim_{L=\infty} \int_0^L [z(x) - m][z(x + \tau) - m]dx = \left[R(\tau) - m^2 \right]/\mu^2$$

Many engineering surfaces are found to have an exponential ACF. The measure of how quickly the random event decays is called the correlation length. The correlation length is the length over which the autocorrelation function drops to small fraction of its value at origin, typically 10% of its original value. The correlation length β^* can be viewed as a measure of randomness. The degree of randomness of a surface increases with an increase in the magnitude of β^*.

A.5 Types of Mechanical Face Seals

A.5.1 Fixed Clearance Seals

The common types of fixed clearance seals are as follows (Lebeck, 1991).

• **Visco Seal**

The visco seal can seal directly against a liquid using the liquid itself or by using a separate supply of liquid, may seal against a gas. The effectiveness of the visco seal depends primarily on the viscosity and clearance.

• **Labyrinth Seal**

This seal relies mainly on creating a high loss leakage path to minimize leakage. This seal can be used for liquids as well as gases.

• **Bushing Seal**

In this seal the flow area is the annulus created between the bushing clearance and the shaft. Resistance to flow is determined by the length and the clearance and the clearance should be large enough to allow for all shaft motion.

• **Floating Ring Seal**

This seal is similar to the bushing seal except that the bushing is allowed to float freely in the radial direction so that shifting the bushing can accommodate large radial motions of the shaft. Thus, the floating ring can have a smaller clearance than the fixed bushing seal.

• **Ferrofluid Seal**

In this a magnetic fluid is held in place by magnets. The fluid can maintain a small pressure difference before it is pushed out of the gap. The magnetic fluid is a suspension of magnetic particles in a liquid. By staging the ferrofluid seal, significant pressure differentials can be handled. The primary advantage of the ferrofluid seal is that there is zero leakage.

A.5.2 Surface Guided Seals

The surface guided seals are classified with respect to the type of guiding surface. Nearly all the rotating shaft seals contact either on an annular surface or a cylindrical surface.

A.5.2.1 Cylindrical Surface

• Lip Seal

The lip seal contacts over a small axial length. This seal is generally not suitable for significant pressure differentials. Most lip seals are of the cylindrical surface guided type.

• Circumferential Seal

This seal contacts on a cylindrical surface over a definite axial length unlike the lip seal. It has some type of segments that allow it to clamp around the cylinder entirely and it may be pressure loaded.

• Packing

Packing itself represents a cylindrical surface guided type of seal. Commonly this seal contacts or partially contacts over a large area.

A.5.2.2 Annular Surface Seals

• Lip Seal

A lip seal can be designed to contact on some small part of an annulus. But the cylindrical geometry is most common.

• Mechanical Face Seal

The mechanical face seal contacts over a significant radial fraction of the annulus. Comparing this seal to its cylindrical surface counter part such as the circumferential seal, it is somewhat simpler because the seal is not made in segments.

A.6 Permeability

Permeability (commonly symbolized as κ or k) is a measure of the ability of a material (typically, a rock or unconsolidated material) to transmit fluids. It is of great importance in determining the flow characteristics of hydrocarbons in oil and gas reservoirs, and of groundwater in aquifers.

The *intrinsic permeability* of any porous material is:

$$k_I = Cd^2$$

where

k_I is the intrinsic permeability [L^2]

C is a dimensionless constant that is related to the configuration of the flow-paths

d is the average, or effective pore diameter [L]

Permeability needs to be measured either directly (using Darcy's law) or through estimation using empirically derived formulas. A common unit for permeability is the *darcy* (D), or more commonly the *millidarcy* (mD) (1 darcy $\approx 10^{-12}$ m^2). Other units are cm^2 and the SI m^2. *Permeability* is part of the proportionality constant in Darcy's law which relates discharge (flow rate) and fluid physical properties (e.g. viscosity) to a pressure gradient applied to the porous media. The proportionality constant specifically for the flow of water through a porous media is the hydraulic conductivity. Permeability is a property of the porous media only, not the fluid.

A.7 Porosity

Porosity is a measure of the void spaces in a material and is measured as a fraction between 0–1 or as a percentage between 0–100%. The term *porosity* is used in multiple fields including manufacturing earth sciences and construction.

Porosity is indirectly related to hydraulic conductivity. For two similar sandy aquifers, the one with a higher porosity will typically have a higher hydraulic conductivity (more open area for the flow of water) but there are many complications to this relationship. Clays, which typically have very low hydraulic conductivity also have very high porosities (due to the structured nature of clay minerals) It means clays can hold a large volume of water per volume of bulk material but they do not release water very quickly. Well sorted (grains of approximately all one size) materials have higher porosity than similarly sized poorly sorted materials (where smaller particles fill the gaps between larger particles). The graphic illustrates how some smaller grains can effectively fill the pores (where all water flow takes place) drastically reducing porosity and hydraulic conductivity while only being a small fraction of the total volume of the material.

Variation of hydrodynamic film force is shown with various frequencies under various permeability of porous rubber in Chapter 3. Permeability is a flow property and is cuased from the porosity and the definite pore size of the materials. Therefore, attention must be given on the relation of permeability with porosity and pore size of the material. This relationship is mostly important in the manufacturing of many engineering materials. The permeability of porous materials can be well approximated by the Blake

Kozeny (1966) equation as $k = \dfrac{r_s^2 \alpha^3}{37.5(1-\alpha)^2}$ where as r_s is mean pore radius and α is

the porosity of matrials. This relationship can be shown as,
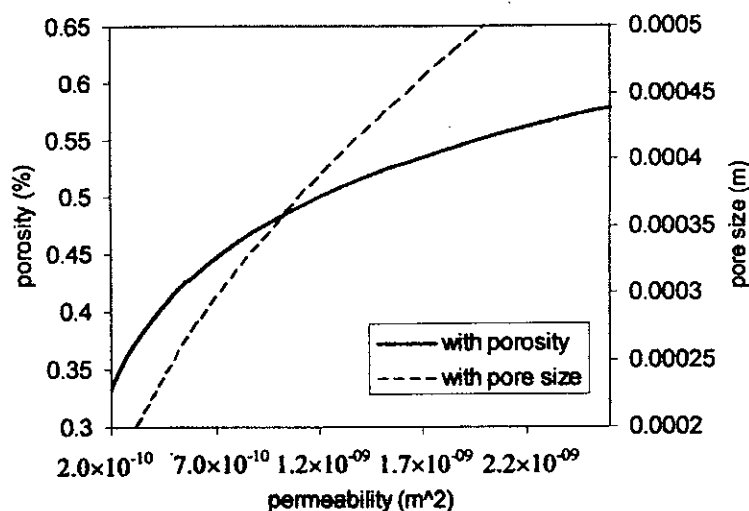
Figure A.4 Relationship of permeability with porosity and pore size

86

Appendix B
Reynolds Equation

B 1. Reynolds Equation

The well known Reynolds equation is one of the fundamental equations used in the field of fluid mechanics. The differential equation governing the pressure distribution in fluid film lubrication was first derived by O. Reynolds in 1886, for incompressible fluid. This was an unnecessary restriction and later the effects of compressibility were included. The Reynolds equation forms the foundation of fluid film theory. This equation establishes a relation between the geometry of the surfaces, relative sliding velocity, the property of the fluid and the magnitude of the normal load the bearing can support.

Before deriving the full equation the assumptions that are to be made must be considered. The assumptions are

1. Body forces are neglected, i.e. there are no extra fields of forces acting on the fluid. This is true except for magnetohydrodynamics.

2. The pressure is constant through the thickness of the film. As the film is only one or two thousandths of a millimeter thick it is always true. With elastic fluids there may be exceptions.

3. Te curvature of surfaces is large compared with film thickness. Surface velocities need not to be considered as varying direction.

4. There is no slip at the boundaries. The velocity of the oil layer adjacent to the boundary is the same as that of the boundary. There has been much work on this and it is universally accepted.

The next assumptions are put in for simplification. They are not necessarily true but without them the equation gets more complex. So the assumptions for further simplification along with the above the assumptions are:

5. The lubricant is Newtonian, i.e. stress is proportional to rate of shear.

6. Flow is laminar. In big turbine bearing it is not true and the theory is being slowly developed.

7. Fluid inertia is neglected. Several studies have shown that even if Reynolds number is 1000 the pressure is only modified by about 5 percent.

8. The viscosity is constant through the film thickness. This is certainly not true but leads the great complexity if it is not assumed.

On the basis of the above assumptions the Reynolds equation is developed.

B 2. Continuity of flow of a column

Consider a column of fluid of height h and base dx, dz (shown in the Figure B.1). Fluid flows into the column from the left at a rate q_x per unit width. The volume flow rate is $(q_x dz)$, for the column of dz wide. The rate of flow per unit width is

$$q_x + \frac{\partial q_x}{\partial x} dx \qquad\qquad (B.1.1)$$

where, $\partial q_x / \partial x$ is the rate of change of flow in the x direction, and the dx is small enough to $\partial q_x / \partial x$ as linear. Here upper plate is assumed as porous plate. So outlet flow along the y-axis $u_{pm} dx dz$ is considered as flow through the porous material.

88

The actual flow out is

$$\left(q_x + \frac{\partial q_x}{\partial x} dx\right) dz \qquad (B.1.2)$$
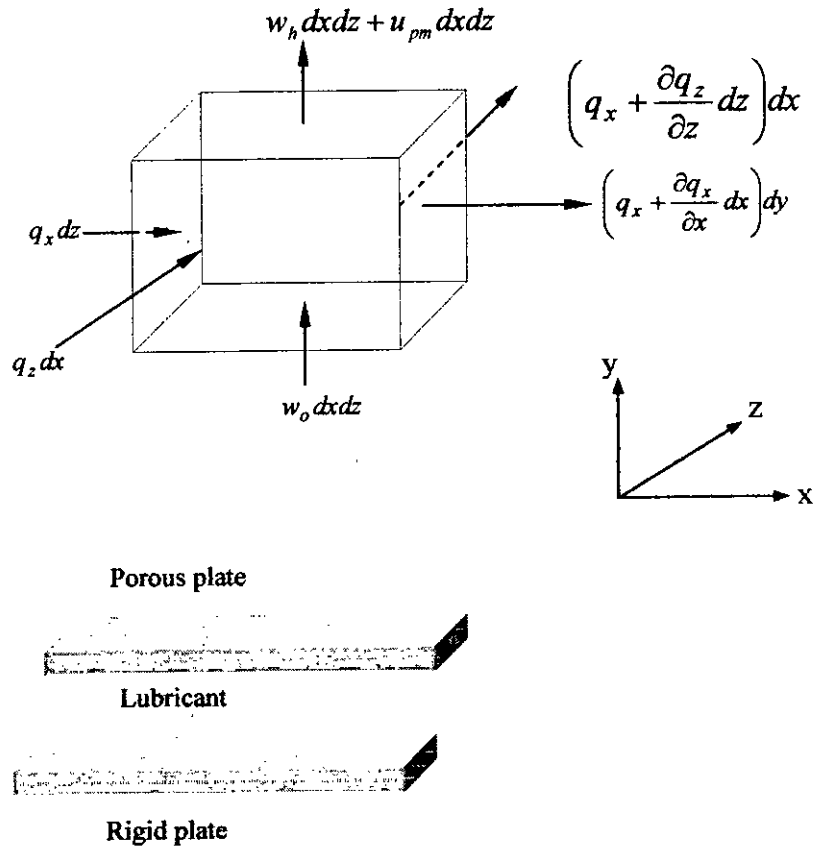
Figure B.1: Continuity of a flow of a fluid element

In the z direction the same argument applies. The flow rate in is $\left(q_x dz\right)$ and out is

$$\left(q_z + \frac{\partial q_z}{\partial z} dz\right) dx \qquad (B.1.3)$$

The vertical flow is rather different. If the floor of the column moves upwards at a velocity w_0 and if the floor moves upwards as well at a speed w_h the volume of the column changes at a rate $(w_h - w_0)dxdz$, where $(dx\ dz)$ is the area both of the base and

of the roof. Although the base and roof are moving, at the instant considered the height is h, through a fraction of time later it will of course have altered.

For the continuity of the flow, the fluid being of constant density, the rate flowing in must equal the rate flowing out. These can all be added up thus. Flowing into the column

$$q_x \, dz + q_z \, dx + w_o \, dx \, dz \tag{B.2}$$

Flowing out of the column

$$\left(q_x + \frac{\partial q_x}{\partial x} dx\right) dz + \left(q_z + \frac{\partial q_z}{\partial z} dz\right) dx + w_h \, dx \, dz + u_{pm} \, dx \, dz \tag{B.3}$$

The equation B.2 and equation B.3 are equal. So equating the equations and after cancellations of the same terms we get:

$$\frac{\partial q_x}{\partial x} dx \, dz + \frac{\partial q_z}{\partial z} dz \, dx + \left(w_h + u_{pm} - w_0\right) dx \, dz = 0 \tag{B.4.1}$$

Now $(dx \, dz)$ is arbitrary and non zero, so canceling the term from the both side yields

$$\frac{\partial q_x}{\partial x} + \frac{\partial q_z}{\partial z} + \left(w_h - w_0\right) + u_{pm} = 0 \tag{B.4.2}$$

In unsteady state conditions the density of the column may change with time, and this must be taken into account. If the density is the same through out the height of the column the analysis leads to:

$$\frac{\partial}{\partial x}\left(\rho q_x\right) + \frac{\partial}{\partial z}\left(\rho q_z\right) + \rho\left(w_h - w_0\right) + \rho u_{pm} = 0 \tag{B.4.3}$$

where ρ is the density of the fluid.

According to the principle of mass conservation the rate at which mass is accumulating in the control volume $\frac{\partial \rho h}{\partial t}$ must be equal to the difference between the rates at which mass enters and leaves. Therefore,

$$-\frac{\partial \rho q_x'}{\partial x} - \frac{\partial \rho q_y'}{\partial y} = \frac{\partial \rho h}{\partial t} \qquad (B.4.4)$$

$$\frac{\partial \rho h}{\partial t} = \rho \frac{\partial h}{\partial t} + h \frac{\partial \rho}{\partial t} \qquad (B.4.5)$$

$$\frac{\partial \rho h}{\partial t} = \rho \left(w_a - w_b - u_a \frac{\partial h}{\partial x} - v_a \frac{\partial h}{\partial y} \right) + h \frac{\partial \rho}{\partial t} \qquad (B.4.6)$$

If upper plate has no slide motion over the lower plate the terms $u_a \frac{\partial h}{\partial x} = 0$ and $v_a \frac{\partial h}{\partial y} = 0$ and in case of incompressible fluid density will not be changed with time. Therefore, the term $\frac{\partial \rho}{\partial t}$ becomes zero. The Eq.(B.4.3) becomes as follows:

$$\frac{\partial}{\partial x}(\rho q_x) + \frac{\partial}{\partial z}(\rho q_z) + \frac{\partial}{\partial t}(\rho h) + \rho u_{pm} = 0 \qquad (B.4.7)$$

As density of fluid remain uniform throughout the fluid film so Eq. (B.4.7) becomes as,

$$\frac{\partial q_x}{\partial x} + \frac{\partial q_z}{\partial z} + \frac{\partial h}{\partial t} + u_{pm} = 0 \qquad (B.5)$$

In cylindrical coordinate this equation becomes as,

$$\frac{1}{r}\frac{\partial(q_r r)}{\partial r} + \frac{1}{r}\frac{\partial q_\theta}{\partial \theta} + \frac{\partial h}{\partial t} + u_{pm} = 0 \qquad (B.5i)$$

B 3. Equilibrium of an element
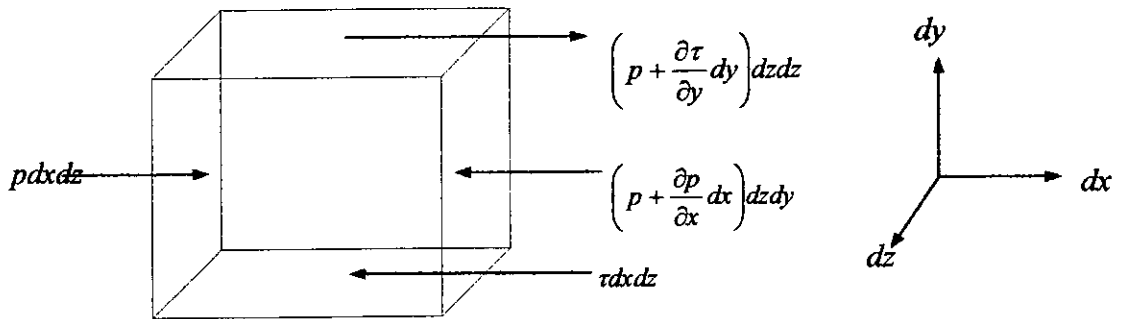
Figure B.2: Equilibrium of an element

Take a small element of fluid of sides $dxdydz$ (shown in the figure B.2) and consider first the forces in the x direction only. On the left of the element there is a pressure p on the face of area $dzdy$, giving a force, acting on the right, of $pdzdy$. On the opposite face the pressure is:

$$p + \frac{\partial p}{\partial x}dx \qquad (B.6.1)$$

The corresponding force is

$$\left(p + \frac{\partial p}{\partial x}dx\right)dz\,dy \qquad (B.6.2)$$

There are shear stresses on the top and bottom faces, producing forces. On the bottom face the shear stress τ gives a force ($\tau\ dx\ dz$) acting on the left and on the top face, and acting to the right, is force

$$\left(\tau + \frac{\partial \tau}{\partial y} dy\right) dx dz \tag{B.6.3}$$

The shear stress on the top face being $\left(\tau + (\partial \tau / \partial y) dy\right)$.

These forces acting to the left and right must balance each other so

$$p\,dz\,dy + \left(\tau + \frac{\partial \tau}{\partial y} dy\right) dx\,dz = p + \frac{\partial p}{\partial x} dz\,dy + \tau\,dx\,dz \tag{B.7.1}$$

Expanding and canceling the common terms from the right and left sides of the above equation yield

$$\frac{\partial \tau}{\partial y} dy\,dx\,dz = \frac{\partial p}{\partial x} dx\,dz\,dy \tag{B.7.2}$$

or, $\qquad \dfrac{\partial \tau}{\partial y} = \dfrac{\partial p}{\partial x}$ $\qquad\qquad$ (B.7.3)

According to Newton's Law of Viscosity

$$\tau = \eta \frac{\partial u}{\partial y} \tag{B.7.4}$$

From the equation (7.c) and equation (8) we can write

$$\frac{\partial p}{\partial x} = \frac{\partial}{\partial y}\left(\eta \frac{\partial u}{\partial y}\right) \tag{B.8}$$

In the y direction the shear stresses and pressure can be equated and a similar equation follows

$$\frac{\partial \tau}{\partial y} = \frac{\partial p}{\partial z} \qquad\qquad (B.9.1)$$

$$\tau = \eta \frac{\partial v}{\partial y} \qquad\qquad (B.9.2)$$

From the equation (8.a) and equation (8.b) we get

$$\frac{\partial p}{\partial z} = \frac{\partial}{\partial y}\left(\eta \frac{\partial v}{\partial y}\right) \qquad\qquad (B.9.3)$$

The pressure gradient in the z direction is zero (by definition), so $\partial p / \partial z = 0$.

Considering the equation (8) that can be integrated since p is not the function of z. Integrating the equation (8) we get

$$\eta \frac{\partial u}{\partial y} = \frac{\partial p}{\partial x} y + C_1 \qquad\qquad (B.10)$$

where C_1 is the integration constant.

Now both η and u are the function of y but it is too difficult to consider both at once so η is taken as constant with respect to y. It is important to realize that this is a important assumption and the assumption is made only for the simplicity. The inclusion of $(d\eta / dy)$ can modify the equation very considerably in certain circumstances.

However, making the assumption, a further integration is performed to the equation and yield

$$\eta u = \frac{\partial p}{\partial x} \frac{y^2}{2} + C_1 y + C_2 \qquad\qquad (B.10.1)$$

According to assumption 4, the boundary conditions are simple as the speed of the fluid at the surface is the speed of the surface it self,

$$y = h, \quad u = U_1 \tag{B.10.2}$$

$$y = 0, \quad u = U_2 \tag{B.10.3}$$

where U_1 and U_2 are the surface speeds

Substituting the boundary conditions in the equation (10.a), we get accordingly

$$C_2 = \eta U_2 \tag{B.10.4}$$

$$C_1 = \frac{\eta(U_1 - U_2)}{h} - \frac{\partial p}{\partial x}\frac{h}{2} \tag{B.10.5}$$

Finally we get equation (10.a) in the following form after substituting the values of constants into that equation

$$u = \frac{\partial p}{2\eta \partial x}\left(y^2 - yh\right) + \left(U_1 - U_2\right)\frac{y}{h} + U_2 \tag{B.11}$$

where $\partial p / \partial x$ is the pressure gradient, η is the viscosity, U_1 and U_2 are the surface speeds on $y = h$ and $y = 0$; and of course from the equation (11) the velocity gradient is

$$\frac{\partial u}{\partial y} = \frac{\partial p}{\eta \partial x}\left(y - \frac{h}{2}\right) + \frac{(U_1 - U_2)}{h} \tag{B.12}$$

Now the integrating the above equation from 0 to h will give the flow rate in the x direction per unit width of z (i.e., $q_x = \int_0^h u \, dy$). By integrating the equation (12) will yield

$$q_x = \left[\frac{\partial p}{2\eta \partial x}\left(\frac{y^3}{3} - \frac{y^2 h}{2}\right) + \left(U_1 - U_2\right)\frac{y^2}{2h} + U_2 y\right]_0^h \tag{B.13}$$

95

Putting the limits and simplifying we get

$$q_x = \frac{-h^3 \partial p}{12\eta \partial x} + (U_1 + U_2)\frac{h}{2} \qquad \text{(B.14)}$$

Following the same procedure we get flow rate in y direction

$$q_z = \frac{-h^3 \partial p}{12\eta \partial z} + (V_1 - V_2)\frac{h}{2} \qquad \text{(B.15)}$$

where V_1 and V_2 correspond to U_1 and U_2. Important assumption for present research is that there is relative motion between the upper plate and the lower plate which leads to the terms U_1, U_2, V_1 and V_2 zero.

B 4. Full Reynolds Equation

Now substituting the expression of q_x and q_y in the equation (B.5) (i.e., continuity equation) yield

$$\frac{\partial}{\partial x}\left(-\frac{h^3 \partial p}{12\eta \partial x}\right) + \frac{\partial}{\partial z}\left(-\frac{h^3 \partial p}{12\eta \partial z}\right) + \frac{\partial h}{\partial t} + u_{pm} = 0 \qquad \text{(B.16)}$$

The comparable equation to (B.16) as expressed in the cylindrical coordinate as Eq. (B.5i) is

$$\frac{1}{r}\frac{\partial}{\partial r}\left(rh^3 \frac{\partial p}{\partial r}\right) + \frac{1}{r}\frac{\partial}{\partial \theta}\left(h^3 \frac{\partial p}{\partial \theta}\right) = 12\eta\left(\frac{\partial h}{\partial t} + u_{pm}\right) \qquad \text{(B.16.1)}$$

For one dimensional Reynolds equation this equation is simplified as

$$\frac{\partial}{\partial r}\left(rh^3 \frac{\partial p}{\partial r}\right) = 12\eta r\left(\frac{\partial h}{\partial t} + u_{pm}\right) \qquad \text{(B.16.2)}$$

In the fluid mechanics of porous media, the place of momentum equations or force balances is occupied by the numerous experimental observations summarized mathematically as the *Darcy law*. These observations were first reported by Darcy who, based on measurement alone, discovered that the area averaged fluid velocity through a column of porous material is directly proportional to the pressure gradient established along the column. Subsequent experiments proved that area-averaged velocity is, in addition, inversely proportional to the viscosity of the fluid seeping through the porous media. According to Darcy law fluid velocity through the porous media,

$$u_{pm} = -\frac{k}{\eta}\frac{\partial p_m}{\partial z}\bigg|_{z=l} \qquad\qquad (B.16.3)$$

In the Darcy's observation the fluid flow direction was from the porous material to the atmosphere. But in the present research phenomenon the flow direction is just opposite to the Darcy's observation. Therefore Eq. (B.16.3) becomes as,

$$u_{pm} = \frac{k}{\eta}\frac{\partial p_m}{\partial z}\bigg|_{z=l} \qquad\qquad (B.16.4)$$

Putting this equation in the Eq. (B.16.2) the modified Reynolds becomes,

$$\frac{\partial}{\partial r}\left(rh^3\frac{\partial p}{\partial r}\right) = 12\eta r\left(\frac{\partial h}{\partial t} + \frac{k}{\eta}\frac{\partial p_m}{\partial z}\bigg|_{z=l}\right) \qquad\qquad (B.17)$$

Appendix C

Computer Code

C.1 Program 1

```
/*      Program to Solve 2-D Reynolds Equation by Finite Difference Technique for
                          solid porous rubber block      */

#include<stdio.h>
#include<conio.h>
#include<malloc.h>
#include<stdlib.h>
#include<iostream.h>
#include<math.h>
int **porous;
float **pm;
float *array;
int row, col;
FILE *out;
float R=0.049,L=0.0065;
int coff1,coff2,coff3;

void func(int a, int b)
{
        int i,j;
        int index=0;
        int flag=0;
        if(b==0)                    //left boundary  (r==0)
        {
                for(int i=0;i<(row*col);i++)
                        array[i]=0;
                int temp=col*a;
                array[temp]=-3;
                array[temp+1]=4;
                array[temp+2]=-1;
        }
        else if(b==(col-1))                    //right boundary  r=ra
        {
                for(int i=0;i<(row*col);i++)
                        array[i]=0;
                int temp=a*col;
                temp=temp+b;
                array[temp]=1;
```

```
}
else if(a==(row-1) && (b!=0 && b!=col))   //top boundary (z==1)
{
        for(int i=0;i<(row*col);i++)
                array[i]=0;
        int temp=a*col;
        temp=temp+b;
        array[temp]=1;
}

else if(a==0 && (b!=0 && b!=col))        //bottom boundary (z==0)
{
        for(j=0;j<row;j++)
        {
                for(i=0;i<b;i++)
                {
                        array[index++]=0;
                }
                if(flag==0)
                        array[index++]=-3;
                else if(flag==1)
                        array[index++]=4;
                else if(flag==2)
                        array[index++]=-1;
                for(i=(b+1);i<col;i++)
                {
                        array[index++]=0;
                }
                flag++;
        }
}
else
{
        for(int i=0;i<(row*col);i++)
        {
                array[i]=0;
        }
        int temp=(col*a)+b;
        float delr=R/(col-1);
        float Rj=delr*(b);
        float delz=L/(row-1);
        array[temp]=-2*(1+((delr/delz)*(delr/delz)));
        array[temp-1]=(1-(delr/(2*Rj)));
        array[temp+1]=(1+(delr/(2*Rj)));
        temp=(col*(a-1))+b;
        array[temp]=((delr/delz)*(delr/delz));
        temp=(col*(a+1))+b;
        array[temp]=((delr/delz)*(delr/delz));
```

```
            }
}
void main()
{
        int i,j;
        float
h[20],radii[20],p[20][20],c[50],cf[50],vrm,c1,c2,vrmsum=0.0,kp,eta,xx[20][20],pf[5
0],h_abs,as,f,t,comp[50],error_r,error_a;              //user
        float
Q,muh,del,del_z,h0[20],add,pt[50],x1[50],sum=0.0,sum1=0.0,ea,er=0.0001,k,x[50],f
actor=0.0;
        float is,is1,is2,is3,is4,cor[20],val;
        int rr,cc,stop=1,m,g,l,num=0;
        //del=R/(col-1);
        clrscr();
        printf("Enter the dimension:");
        scanf("%d%d",&row,&col);
        /************************initilization********************/
        del=R/(col-1);
        del_z=L/(row-1);
        c1=5.568*del*del;
        c2=(0.000000006312*((del*del)/del_z));
        kp=0.000000000263;
        eta=0.116;
        h_abs=0.0014;
        as=0.0003;
        f=20;
        error_r=0.0001;
        for(i=0;i<(col-1);i++)
        { comp[i]=20.0;}
         comp[col-1]=0.0;
        for(i=0;i<col;i++)
        {
                h[i]=0.0035;
                radii[i]=del*i;
                h0[i]=8.5;
        }
        for(i=0;i<(row*col);i++)
          {
                c[i]=0.0;
          }
        for(i=(((row-1)*col)+1);i<(row*col-1);i++)
          {
                c[i]=20000.0;
          }
        for(i=0;i<row;i++)
        { cor[i]=0.0;
        }
```

```
/*********************end initilization**********************/
    m=0;
    porous=(int **)malloc(row*sizeof(int *));
    for(i=0;i<row;i++)
    {
            porous[i]=(int *)malloc(col*sizeof(int));
    }
    pm=(float **)malloc((row*col)*sizeof(float *));
    for(i=0;i<(row*col);i++)
    {
            pm[i]=(float *)malloc((row*col)*sizeof(float));
    }
    array=(float *)malloc((row*col)*sizeof(float));
    out=fopen("out.txt","w+");
    if(out==NULL)
    {
            printf("Error in opening file\n");
            exit(1);
    }
    for(i=0;i<row;i++)
    {
            for(j=0;j<col;j++)
            {
                    func(i,j);
        //      for(int k=0;k<(row*col);k++)
                    //fprintf(out,"%0.2f ",array[k]);
                    //fprintf(out,"\n");
            }
    }
    int index=0;
    for(i=0;i<row;i++)
    {
            for(j=0;j<col;j++)
            {
                    func(i,j);
                    for(int k=0;k<(row*col);k++)
                    {
                            pm[index][k]=array[k];
        //              fprintf(out,"%0.2f",array[k]);
                    }
                    index++;
        //      fprintf(out,"\n");
            }
    }

    // fprintf(out,"transferred matrix are:\n");
/***************start of time loop*****************************/
    for(t=0.0001;t<=0.1;t=t+0.0002)
```

```
{
for(l=0;l<500;l++)
{
 m=0;
 sum=0.0;
 sum1=0.0;
 er=0.0001;
 factor=0.0;

 for(i=0;i<(row*col);i++)
 {
         x[i]=0.0;
 }
 x[1]=1.0;
 for(k=1;k<1000;k++)              //matrix solver for porous pressure
{   m=0;
 for(i=0;i<(row*col);i++)
 {
         factor=x[i];
         for(j=0;j<=i-1;j++)
         {
                 sum=sum+pm[i][j]*x[j];
         }
         for(j=i+1;j<(row*col);j++)
         {
                 sum1=sum1+pm[i][j]*x[j];
         }
         x[i]=(1.0/pm[i][i])*(c[i]-sum-sum1);

         ea=(x[i]-factor)/100.0;
         if(ea<0.0) ea=-1.0*ea;
         if(ea<er) m++;
         ea=0.0;
         sum=0.0;
         sum1=0.0;
 }
 if(m>=(row*col)) break;
 m=0;
 sum=0.0;
 sum1=0.0;
}
         cc=0;
         for(i=0;i<row;i++)
         { for(rr=0;rr<col;rr++)
                 { xx[i][rr]=x[cc];
                   cc++;
                 }
         }
```

```
          cc=0;
          add=0.0;
          for(rr=0;rr<col;rr++)
          {  for(i=1;i<(row-1);i++)
                    {add=add+xx[i][rr];
                    }
            x1[rr]=(xx[0][rr]+2.0*add+xx[row-1][rr])/(2.0*(row-1));
            add=0.0;
            }
/***************porous solution end************************/
 vrmsum=0.0;
 for(i=1;i<=(col-2);i++)
 { vrmsum=vrmsum+radii[i]*(h0[i]+(kp/eta)*(3*xx[row-1][i]-4*xx[row-
2][i]+xx[row-3][i])/(2.0*del_z));
 }
 vrm=-(1.0/(h_abs+as*(cos(2.0*3.1416*f*t)-1.0)+(pt[col-1]*L/6080000.0)*(1.0-
0.45733*exp(-218.81*t))))*(1.0/(2.0*(col-1)))*(2*vrmsum+R*(h0[col-
1]+(kp/eta)*(3*xx[row-1][col-1]-4*xx[row-2][col-1]+xx[row-3][col-
1])/(2.0*del_z)));
 cf[0]=0.0;
 if(vrm<0)cf[col-1]=-((970.0*1.5*vrm*vrm)/2.0);
 else if(vrm>=0)cf[col-1]=0.0;
 vrmsum=0.0;
 for(rr=1;rr<(col-1);rr++)
 { cf[rr]=1.0*((c1*radii[rr]*h0[rr])+(c2*radii[rr])*(3.0*xx[row-1][rr]-4.0*xx[row-
2][rr]+xx[row-3][rr]));
 }
/****************end condition for reynolds******************/
 cc=0;
 rr=0;
 for(i=0;i<col;i++)                              //front bc
 {
          p[rr][i]=0.0;
 }
 p[rr][cc]=-3.0;
 p[rr][cc+1]=4.0;
 p[rr][cc+2]=-1.0;


                                                 //last bc
 for(i=0;i<col;i++)
 {
          p[col-1][i]=0.0;
 }
 p[col-1][col-1]=1.0;
 for(rr=1;rr<(col-1);rr++)
 {
          for(i=0;i<col;i++)
          {
```

```
                        p[rr][i]=0.0;
            }
            p[rr][rr]=(-4.0*radii[rr+1]*h[rr+1]*h[rr+1]*h[rr+1])+(-4.0*radii[rr-1]*h[rr-
1]*h[rr-1]*h[rr-1]);
            p[rr][rr-1]=1.0*radii[rr+1]*h[rr+1]*h[rr+1]*h[rr+1]+(3.0*radii[rr-1]*h[rr-
1]*h[rr-1]*h[rr-1]);
            p[rr][rr+1]=3.0*radii[rr+1]*h[rr+1]*h[rr+1]*h[rr+1]+(1.0*radii[rr-1]*h[rr-
1]*h[rr-1]*h[rr-1]);


    }
            ea=0.0;
            sum=0.0;
            sum1=0.0;
            m=0;
            for(k=0;k<col;k++)
            { pf[i]=0.0;
            }
            pf[0]=1.0;
    for(k=1;k<1000;k++)                    //matrix solver for film pressure
{   m=0;
  for(i=0;i<col;i++)
  {
            factor=pf[i];
            for(j=0;j<=i-1;j++)
            {
                    sum=sum+p[i][j]*pf[j];
            }
            for(j=i+1;j<col;j++)
            {
                    sum1=sum1+p[i][j]*pf[j];
            }
            pf[i]=(1.0/p[i][i])*(cf[i]-sum-sum1);

            ea=(pf[i]-factor)/100.0;
            if(ea<0.0) ea=-1.0*ea;
            if(ea<er) m++;
            ea=0.0;
            sum=0.0;
            sum1=0.0;
            }
            if(m>=(col-1)) break;
            m=0;
            sum=0.0;
            sum1=0.0;
}
/***********************solution end for film pressure******************/
  for(rr=0;rr<col;rr++)
  {pt[rr]=(x1[rr]+pf[rr]);}
```

```c
for(rr=0;rr<col;rr++)
{ h[rr]=(h_abs+as*(cos(2.0*3.1416*f*t)-1.0)+(pt[rr]*L/6080000.0)*(1.0-
0.45733*exp(-218.81*t)));
    h0[rr]=-
2.0*3.1416*f*as*sin(2.0*3.1416*f*t)+(pt[rr]*L/6080000.0)*((0.45733/0.00457)*ex
p(-218.81*t));
}
/*********************end value for h and h0*********************/
m=0;
for(i=0;i<col*row;i++)
{ error_a=0.0;
      error_a=pf[i]-comp[i];
      if(error_a<0)error_a=-1.0*error_a;
      if(error_a<=error_r)m++;

}
/*********************end convergence checking*********************/

for(i=0;i<row;i++)
{ val=pf[i]-cor[i];
  if(val<0)val=val*(-1);
  if(val<0.001)num=num+1;
}

for(i=0;i<(row*col);i++)
      {
        c[i]=0.0;
      }
g=1;

for(i=(((row-1)*col)+1);i<(row*col-1);i++)
      { c[i]=pf[g];
            g=g+1;
      }
  for(i=0;i<row;i++)
  { cor[i]=pf[i];
  }
  if(num==col){ num=0; break;}
  num=0; val=0.0;
  }
/*********************results*********************/
/*********************leakage flow rate*********************/
/*Q=2.0*3.1416*R*(0.0014+as*(cos(2.0*3.1416*f*t)-1.0)+(pt[col-
1]*L/6080000.0)*(1.0-0.45733*exp(-218.81*t)))*vrm;
fprintf(out,"%.15f\n ",Q);
printf("%.15f=\n ",Q);*/
/*********************hydrodynamic film force*********************/
/*is=0.0;
```

```c
is1=0.0;
is2=0.0;
for(i=1;i<(col-1);i++)
{is1=is1+pf[i]*radii[i];
}
is2=radii[col-1]*(pf[0]*radii[0]+2.0*is1+pf[col-1]*radii[col-1])/(2.0*(col-1));
is=(2.0*3.1416*is2);
fprintf(out,"%.17f\n",is);
printf("%.17f\n",is);
is=0.0;
is1=0.0;
is2=0.0; */
/*****************pressure at center******************************/
fprintf(out,"%.15f\n ",pf[0]);
printf("%.15f=\n ",pf[0]);


}
/***********************end of convergence loop******************/

        fclose(out);
        getch();
}
```

C.2 Program 2

```
/*  Program to Solve 2-D Reynolds Equation by Finite Difference Technique for
           annular porous rubber block considering rough surface */

#include<stdio.h>
#include<conio.h>
#include<malloc.h>
#include<stdlib.h>
#include<iostream.h>
#include<math.h>
int **porous;
float **pm;
float *array;
int row, col;
FILE *out;
float Ro=0.00839,Ri=0.0016067,L=0.00046325;// small specimen
int coff1,coff2,coff3;

void func(int a, int b)
{
        int i,j;
        int index=0;
        int flag=0;
        if(b==0)                //left boundary  (r==0)
        {
                for(int i=0;i<(row*col);i++)
                        array[i]=0;
                int temp=col*a;
                array[temp]=1.0;
                //array[temp+1]=4;
                //array[temp+2]=-1;
        }
        else if(b==(col-1))                //right boundary  r=ra
        {
                for(int i=0;i<(row*col);i++)
                        array[i]=0;
                int temp=a*col;
                temp=temp+b;
                array[temp]=1;
        }
        else if(a==(row-1) && (b!=0 && b!=col))   //top boundary (z==1)
        {
                for(int i=0;i<(row*col);i++)
                        array[i]=0;
                int temp=a*col;
                temp=temp+b;
                array[temp]=1;
```

107

```c
                }
        else if(a==0 && (b!=0 && b!=col))       //bottom boundary (z==0)
        {
                for(j=0;j<row;j++)
                {
                        for(i=0;i<b;i++)
                        {
                                array[index++]=0;
                        }
                        if(flag==0)
                                array[index++]=-3;
                        else if(flag==1)
                                array[index++]=4;
                        else if(flag==2)
                                array[index++]=-1;
                        for(i=(b+1);i<col;i++)
                        {
                                array[index++]=0;
                        }
                        flag++;
                }
        }
        else
        {
                for(int i=0;i<(row*col);i++)
                {
                        array[i]=0;
                }
                int temp=(col*a)+b;
                float delr=(Ro-Ri)/(col-1);
                float Rj=delr*(b);
                float delz=L/(row-1);
                array[temp]=-2*(1+((delr/delz)*(delr/delz)));
                array[temp-1]=(1-(delr/(2*Rj)));
                array[temp+1]=(1+(delr/(2*Rj)));
                temp=(col*(a-1))+b;
                array[temp]=((delr/delz)*(delr/delz));
                temp=(col*(a+1))+b;
                array[temp]=((delr/delz)*(delr/delz));
        }
}
void main()
{
        int i,j;
        float
h[20],radii[20],p[20][20],c[50],cf[50],vrm,c1,c2,vrmsum=0.0,kp,eta,xx[20][20],pf[5
0],h_abs[20],as,f,t,comp[50],error_r,error_a;                    //user
```

108

```c
float
Q,muh,del,del_z,h0[20],add,pt[50],x1[50],sum=0.0,sum1=0.0,ea,er=0.0001,k,x[50],f
actor=0.0;
        int rr,cc,stop,m,g,l,num=0;
        float is,is1,is2,is3,is4,cor[20],val;
        //del=R/(col-1);
        clrscr();
        printf("Enter the dimension:");
        scanf("%d%d",&row,&col);
/***********************initilization********************/
        del=(Ro-Ri)/(col-1);
        del_z=L/(row-1);
        c1=5.568*del*del;
        c2=(0.000000006312*((del*del)/del_z));
        kp=0.000000000263;
        eta=0.116;
/*******************data for rough surface*****************/
        h_abs[0]=0.00149728;
        h_abs[1]=0.00136374;
        h_abs[2]=0.00142392;
        h_abs[3]=0.00132114;
        h_abs[4]=0.00132788;
        h_abs[5]=0.00125296;
        h_abs[6]=0.00132260;
        h_abs[7]=0.00140070;
        h_abs[8]=0.00133594;
        h_abs[9]=0.00142382;
        h_abs[10]=0.00136124;
        h_abs[11]=0.00136304;
/*********************end data*********************/
        as=0.0003;
        f=20;
        error_r=0.0001;
        for(i=0;i<(col-1);i++)
        { comp[i]=20.0;}
          comp[col-1]=0.0;
        for(i=0;i<col;i++)
        {
                h[i]=0.0035;
                radii[i]=Ri+del*i;
                h0[i]=8.5;
        }
        for(i=0;i<(row*col);i++)
          {
                c[i]=0.0;
          }
        for(i=(((row-1)*col)+1);i<(row*col-1);i++)
          {
```

```c
                c[i]=20000.0;
    }
    for(i=0;i<row;i++)
    { cor[i]=0.0;
    }
/*********************end initilization************************/
    m=0;
    porous=(int **)malloc(row*sizeof(int *));
    for(i=0;i<row;i++)
    {
            porous[i]=(int *)malloc(col*sizeof(int));
    }
    pm=(float **)malloc((row*col)*sizeof(float *));
    for(i=0;i<(row*col);i++)
    {
            pm[i]=(float *)malloc((row*col)*sizeof(float));
    }
    array=(float *)malloc((row*col)*sizeof(float));
    out=fopen("out.txt","w+");
    if(out==NULL)
    {
            printf("Error in opening file\n");
            exit(1);
    }
    for(i=0;i<row;i++)
    {
            for(j=0;j<col;j++)
            {
                    func(i,j);
        //      for(int k=0;k<(row*col);k++)
        //              fprintf(out,"%0.2f ",array[k]);
                    //fprintf(out,"\n");
            }
    }
    int index=0;
    for(i=0;i<row;i++)
    {
            for(j=0;j<col;j++)
            {
                    func(i,j);
                    for(int k=0;k<(row*col);k++)
                    {
                            pm[index][k]=array[k];
            //              fprintf(out,"%0.2f",array[k]);
                    }
                    index++;
        //      fprintf(out,"\n");
            }
```

110

```
        }

        // fprintf(out,"transferred matrix are:\n");
    /***************start of time loop********************************/
        for(t=0.0001;t<=0.1;t=t+0.0002)
        { //cout<<endl;
        for(l=0;l<1000;l++)
        {
          m=0;
          sum=0.0;
          sum1=0.0;
          er=0.0001;
          factor=0.0;

          for(i=0;i<(row*col);i++)
          {
                x[i]=0.0;
          }
          x[1]=1.0;
          for(k=1;k<1000;k++)          //matrix solver for porous pressure
{    m=0;
  for(i=0;i<(row*col);i++)
  {
          factor=x[i];
          for(j=0;j<=i-1;j++)
          {
             sum=sum+pm[i][j]*x[j];
          }
          for(j=i+1;j<(row*col);j++)
          {
                sum1=sum1+pm[i][j]*x[j];
          }
          x[i]=(1.0/pm[i][i])*(c[i]-sum-sum1);

          ea=(x[i]-factor)/100.0;
          if(ea<0.0) ea=-1.0*ea;
          if(ea<er) m++;
          ea=0.0;
          sum=0.0;
          sum1=0.0;
          }
          if(m>=(row*col)) break;
          m=0;
          sum=0.0;
          sum1=0.0;
}

          cc=0;
          for(i=0;i<row;i++)
```

```
        { for(rr=0;rr<col;rr++)
                { xx[i][rr]=x[cc];
                  cc++;
                }
        }
        cc=0;
        add=0.0;
        for(rr=0;rr<col;rr++)
        { for(i=1;i<(row-1);i++)
                {add=add+xx[i][rr];
                }
        x1[rr]=(xx[0][rr]+2.0*add+xx[row-1][rr])/(2.0*(row-1));
        add=0.0;
        }
/***************porous solution end***********************/
 for(i=1;i<=(col-2);i++)
 { vrmsum=vrmsum+radii[i]*(h0[i]+(kp/eta)*(3*xx[row-1][i]-4*xx[row-
2][i]+xx[row-3][i])/(2.0*del_z));
 }
 vrm=-((1.0*(Ro-Ri))/((Ro+Ri)*(h_abs[col-1]+as*(cos(2.0*3.1416*f*t)-
1.0)+(pt[col-1]*L/6080000.0)*(1.0-0.45733*exp(-218.81*t)))))*(1.0/(2.0*(col-
1)))*(2*vrmsum+Ri*(h0[0]+(kp/eta)*(3*xx[row-1][0]-4*xx[row-2][0]+xx[row-
3][0])/(2.0*del_z))+Ro*(h0[col-1]+(kp/eta)*(3*xx[row-1][col-1]-4*xx[row-2][col-
1]+xx[row-3][col-1])/(2.0*del_z)));
 //cf[0]=0.0;
 if(vrm<0)
 {
 cf[0]=-((970.0*1.5*vrm*vrm)/2.0);
 cf[col-1]=-((970.0*1.5*vrm*vrm)/2.0);
 }
 else if(vrm>=0)
 {
 cf[0]=0.0;
 cf[col-1]=0.0;
 }
 vrmsum=0.0;
 for(rr=1;rr<(col-1);rr++)
 { cf[rr]=1.0*((c1*radii[rr]*h0[rr])+(c2*radii[rr])*(3.0*xx[row-1][rr]-4.0*xx[row-
2][rr]+xx[row-3][rr]));
 }
/***************end condition for reynolds******************/
 cc=0;
 rr=0;
 for(i=0;i<col;i++)                          //front bc
 {
         p[rr][i]=0.0;
 }
 p[rr][cc]=1.0;
```

```
//p[rr][cc+1]=4.0;
//p[rr][cc+2]=-1.0;


                                                //last bc
for(i=0;i<col;i++)
{
        p[col-1][i]=0.0;
}
p[col-1][col-1]=1.0;
for(rr=1;rr<(col-1);rr++)
{
        for(i=0;i<col;i++)
        {
                p[rr][i]=0.0;
        }
        p[rr][rr]=(-4.0*radii[rr+1]*h[rr+1]*h[rr+1]*h[rr+1])+(-4.0*radii[rr-1]*h[rr-
1]*h[rr-1]*h[rr-1]);
        p[rr][rr-1]=1.0*radii[rr+1]*h[rr+1]*h[rr+1]*h[rr+1]+(3.0*radii[rr-1]*h[rr-
1]*h[rr-1]*h[rr-1]);
        p[rr][rr+1]=3.0*radii[rr+1]*h[rr+1]*h[rr+1]*h[rr+1]+(1.0*radii[rr-1]*h[rr-
1]*h[rr-1]*h[rr-1]);

}
        ea=0.0;
        sum=0.0;
        sum1=0.0;
        m=0;
        for(k=0;k<col;k++)
        { pf[i]=0.0;
        }
        pf[0]=1.0;
 for(k=1;k<1000;k++)                    //matrix solver for film pressure
{   m=0;
 for(i=0;i<col;i++)
 {
        factor=pf[i];
        for(j=0;j<=i-1;j++)
        {
                sum=sum+p[i][j]*pf[j];
        }
        for(j=i+1;j<col;j++)
        {
                sum1=sum1+p[i][j]*pf[j];
        }
        pf[i]=(1.0/p[i][i])*(cf[i]-sum-sum1);

        ea=(pf[i]-factor)/100.0;
        if(ea<0.0) ea=-1.0*ea;
```

```
            if(ea<er) m++;
            ea=0.0;
            sum=0.0;
            sum1=0.0;
            }
            if(m>=(col-1)) break;
            m=0;
            sum=0.0;
            sum1=0.0;
}
}
/*********************solution end for film pressure*****************/
  for(rr=0;rr<col;rr++)
  {pt[rr]=(x1[rr]+pf[rr]);}
  for(rr=0;rr<col;rr++)
  { h[rr]=(h_abs[rr]+as*(cos(2.0*3.1416*f*t)-1.0)+(pt[rr]*L/6080000.0)*(1.0-
0.45733*exp(-218.81*t)));
          h0[rr]=-
2.0*3.1416*f*as*sin(2.0*3.1416*f*t)+(pt[rr]*L/6080000.0)*((0.45733/0.00457)*ex
p(-218.81*t));
  }
/*********************end value for h and h0*********************/
m=0;
for(i=0;i<col*row;i++)
{ error_a=0.0;
          error_a=pf[i]-comp[i];
          if(error_a<0)error_a=-1.0*error_a;
          if(error_a<=error_r)m++;


}
/*********************end convergence checking*******************/
for(i=0;i<row;i++)
{ val=pf[i]-cor[i];
  if(val<0)val=val*(-1);
  if(val<0.001)num=num+1;
}

for(i=0;i<(row*col);i++)
        {
          c[i]=0.0;
        }
g=1;

for(i=(((row-1)*col)+1);i<(row*col-1);i++)
        { c[i]=pf[g];
                g=g+1;
        }
for(i=0;i<row;i++)
  { cor[i]=pf[i];
```

```c
    }
if(num==col){ num=0; break;}
num=0; val=0.0;
}
/********************pressure********************************/
//fprintf(out,"%.15f\n ",pf[0]);
//printf("%.15f=\n ",pf[0]);
/*******************hydrodynamic film force******************/
is=0.0;
is1=0.0;
is2=0.0;
for(i=1;i<(col-1);i++)
{is1=is1+pf[i]*radii[i];
}
is2=radii[col-1]*(pf[0]*radii[0]+2.0*is1+pf[col-1]*radii[col-1])/(2.0*(col-1));
is=(2.0*3.1416*is2);
fprintf(out,"%.9f\n",is);
printf("%.9f\n",is);
is=0.0;
is1=0.0;
is2=0.0;
/**************************leakage flowrate*********************/
//Q=1000000.0*2.0*3.1416*(Ro)*(0.0014+as*(cos(2.0*3.1416*f*t)-1.0)+(pt[col-
1]*L/6080000.0)*(1.0-0.45733*exp(-218.81*t)))*vrm;
//fprintf(out,"%.15f\n ",Q);
//printf("%.15f=\n ",Q);
/**************************pressure profile*********************/

//fprintf(out,"%.5f\n%.5f\n%.5f\n%.5f\n%.5f\n%.5f\n%.5f\n%.5f\n%.5f\n%.5f\n%.5f
\n%.5f\n",pf[0],pf[1],pf[2],pf[3],pf[4],pf[5],pf[6],pf[7],pf[8],pf[9],pf[10],pf[11]);

//printf("%.5f\n%.5f\n%.5f\n%.5f\n%.5f\n%.5f\n%.5f\n%.5f\n%.5f\n%.5f\n%.
5f\n",pf[0],pf[1],pf[2],pf[3],pf[4],pf[5],pf[6],pf[7],pf[8],pf[9],pf[10],pf[11]);
/*****************pressure at center****************************/ .


}
/**********************end of convergence loop*****************/

        fclose(out);
        getch();
}
```

115